Monitoring Vegetation Dynamics in Zhongwei, an Arid City of Northwest China

Haitao Wang

Thesis submitted to the Faculty of the
Virginia Polytechnic Institute and State University
in partial fulfillment of the requirements for the degree of

MASTER OF SCIENCE
IN
GEOGRAPHY

Lisa M. Kennedy, Chair
Yang Shao, Co-chair
Valerie Anne Thomas
Luke Juran

May 7, 2014
Blacksburg, Virginia

Keywords: Urbanization, Vegetation dynamics, Dark Object Subtraction (DOS), Random Forest, Sub-pixel mapping

Monitoring Vegetation Dynamics in Zhongwei, an Arid City of Northwest China

Haitao Wang

Abstract

This case study used Zhongwei City in northwest China to quantify the urbanization and revegetation processes (1990–2011) through a unified sub-pixel measure of vegetation cover. Research strategies included: (1) Conduct sub-pixel vegetation mapping (1990, 1996, 2004, and 2011) with Random Forest (RF) algorithm by integrating high (OrbView-3) and medium spatial resolution (Landsat TM) data; (2) Examine simple Dark Object Subtraction (DOS) atmospheric correction method to support temporal generalization of sub-pixel mapping algorithm; (3) And characterize patterns of vegetation cover dynamics based on change detection analysis.

We found the RF algorithm, combined with simple DOS, showed good generalization capability for sub-pixel vegetation mapping. Predicted sub-pixel vegetation proportions were consistent for "Pseudo-invariant" pixels. Vegetation change analysis suggested persistent urban development within the city boundary, accompanied by a continuous expansion of revegetated area at the city fringe. Urban development occurred at both the suburban and urban core areas, and was mainly shaped by transportation networks. A transition in revegetation practices was documented: the large-scale governmental revegetation programs were replaced by the commercial afforestation conducted by industries. This study showed a slight increase in vegetation cover over the time period, balanced by losses to urban expansion, and a likely severe degradation of vegetation cover due to conversion of arable land to desert vegetation. The loss of arable land and the growth of artificial desert vegetation have yielded a dynamic equilibrium in terms of overall vegetation cover during 1990 to 2011, but in the long run vegetation quality is certainly reduced.

Dedication

I dedicate this thesis to the memory of my parents, Jianping Wang and Wenlan Wang.

I miss you every day.

Acknowledgements

I would like to begin with thanking my advisors, Dr. Lisa M. Kennedy and Yang Shao, for continued support and advice in all of the aspects of this project, and for providing me this opportunity to enhance myself professionally and intellectually. I would like to express my thanks to the members of my committee – Drs. Lisa M. Kennedy, Yang Shao, Valerie Anne Thomas, and Luke Juran – for their many thoughtful comments, and for their gracious consideration in helping this research go forward. I would like to give thanks to the faculty and graduate students at Virginia Tech Geography Department. I am especially grateful to Dr. James B. Campbell who offered insightful advices on this topic.

Table of Contents

List of Figures

List of Tables

Chapter 1: Introduction

1.1 Desertification, revegetation and urbanization

China is one of the countries with a vast area suffering from land desertification and sand encroachment in the world (Shi et al., 2005; Zhu, 1989). The nationwide desertified land area was 2,623,700 square kilometers, taking up 27.33% of national territory (State Forestry Administration, P. R. China, 2011), including much of arid/semiarid north and northwest China. Desertification has long been threatening the nation's environmental security and sustainable socio-economic development, and is considered as one of the most severe environmental problems of China (Fullen and Mitchell 1994; Chen and Tang 2005; Wang *et al.* 2007; Yang, Lan, and Wu 2010). Consequently, Chinese government has made tremendous efforts in combating desertification and sand encroachment since 1950s. A number of key programs on prevention and control of desertification have been initiated in provinces with most severe desertification (Zhu, 1989), and extensive local and regional revegetation projects have been implemented aiming at halting desert encroachment and reconverting desertified land to productive uses. Such initiatives have achieved some success in improving vegetation coverage and fixing sand dunes in desert margin, such as in Mu Us Sandy Land and Tengger Desert (Fullen & Mitchell, 1994; Yang et al., 2010). Nowadays, more emphases were made in desertification monitoring and evaluation. During 1994 to 2011, four national monitoring surveys for desertification and sand encroachment were carried out by the State Forestry Administration of China, so as to estimate the status and dynamics of desertified land for the entire territory (State Forestry Administration, P. R. China, 2011).

Urban areas in the arid/semiarid northwest China have experienced significant change since late 1970s. Although the physical growth of urban areas in the northwest China is not as

fast as those of major cities in the east and southeast China, the urbanized areas are usually the already fragile and supply-limited agricultural lands. Many urban areas/human settlements in the northwest China are also facing severe problems of desertification, droughts, dust storms, and water resource sustainability (Cao, 2008; Shi et al., 2005). At the regional scale, the estimated annual desertification rates increased from 1,560km^2 in 1970s to 3,600 km^2 after 1998 (Wang, Wu, Xue, Sun, & Chen, 2004). To combat desertification, sand encroachment, and dust storms, the Chinese Central Government has implemented several national afforestation programs (*e.g.*, Three North Shelter Forest System Project) to increase forest coverage (Wang, Zhang, Hasi, & Dong, 2010; Zhu, 1989). Extensive regional and local revegetation programs have also been implemented. Many of these programs focused on constructing tree/vegetation belt to control the expansion of deserts and fix sand dunes, and it is not uncommon to see reclamation of desert lands through the expansion of woody vegetation (Wang et al., 2007). For most cities in arid/semiarid northwest China, neither urbanization nor revegetation process has been closed monitored and assessed. Urban remote sensing in China often favors mega-cities such as Beijing, Shanghai, and Guangzhou (Schneider, Seto, & Webster, 2005). Quantitative measures on afforestation or revegetation programs are rarely reported and results can be controversial (Cao, 2008; Ma, 2004).

For major cities in the arid and semi-arid southwestern United States, vegetation cover, general land cover types, and their dynamics have been routinely mapped and monitored, since many of those cities are identified as the fastest growing cities of the US over the last several decades (Wu, 2011). Long-Term Ecological Research (LTER) site has been developed at selected city (*i.e.*, Phoenix) to understand urban growth pattern, population change, climate variability, ecological issues and their interactions and feedbacks (Brazel, Selover, Vose, &

Heisler, 2000). Similarly, fast growing urban areas in Egypt and Saudi Arabia have received considerable attention from remote sensing and land use/cover change perspectives (Shalaby & Tateishi, 2007). Urbanization, agricultural intensification, desertification combined to generate complex land use and land cover patterns and change trajectories, which provide a challenging but interesting setting to study human-environment interactions in arid region (Shalaby, Ghar, & Tateishi, 2004). The spatial-temporal variability of vegetation cover, derived from remote sensing data, would provide valuable index to improve the understanding of the relationships between land cover changes, surface biophysical processes, and socioeconomic consequences.

1.2 Zhongwei city: a desert oasis

Some of China's initial revegetation efforts on desert reclamation were conducted in Ningxia Hui Autonomous Region (*abbr.* Ningxia) which is one of eight provinces with most severe desertification (Fullen & Mitchell, 1994). In particularly, most pioneering works were carried out in Zhongwei County (now Zhongwei City) in southern Ningxia. Zhongwei lies at the edge of oasis in arid area of northwestern region, abuts the southeastern frontier of the Tengger Desert which is the fourth largest desert in China. Its administrative region encompasses a municipal district settled in the alluvial plain of the Yellow River, and two townships that are mainly in rural mountainous area (Wu, 2013). Zhongwei is a place of long history being named in 1399 of Ming Dynasty (Feng, Fan, Lu, & Feng, 1998), before that, the desertification here has been documented for a thousand years (Yang, Lan, and Wu 2010). Centuries of overgrazing and forest destruction caused severe land degradation in this area where the small margin of symbiosis between human and nature stands in a delicate balance. From 1950s, in the need of protecting the Yellow River and the 40 km of railway from sand storm encroachment in Zhongwei, the central and local governments have poured huge expenditure, ambitious and

innovative efforts in combating desertification, which are exceptional rare in the world (Wang et al., 2007; Yang et al., 2010). In recent decades, many natural rehabilitation projects have been carried out in the periphery of city to restrain sand dune movement (Feng et al., 1998; Jiang, 2004; UNDP, n.d.; Wang et al., 2007). The settlement of world-renowned Shapotou Desert Experimental Research Station as well as the development of Shapotou National Nature Reserve (China's first nature reserve for desert ecosystem and artificial vegetation) exemplifies these previous endeavors in desert reclamation.

The vegetation dynamics in Zhongwei has gained high attention in numerous studies. However, many of them focused on an ecological perspective, like ecosystem restoration, ecological engineering or plant physiology, while land cover studies based on remotely sensed data are extremely scanty (Liu, 2012; Shao, 2011; Yan, Wang, Feng, & Wang, 2003). Almost all these studies were reported in Chinese thus have weakened impact and limited scientific audiences. On the other hand, a significant urban growth of Zhongwei within the city has been witnessed during recent decades. Such circumstances make Zhongwei become a good study area for assessment of China's efforts on combating desertification in a view of vegetation cover dynamics. Besides, Zhongwei gives a concentrated glimpse of small and medium-sized cities in this region in terms of patterns and rates of land use / land cover change. Moreover, it provides an opportunity to examine desertification, urbanization, and revegetation – three most representative processes on the Earth's surface caused by human activities – in one place.

1.3 Subpixel image analysis

Remote sensing-based urban vegetation mapping has a long history, particularly using medium spatial resolution data such as those from Landsat series of sensors (Ridd, 1995; Small, 2001; Song, 2005; Wu & Murray, 2003). However, the application of conventional per-pixel

image analysis with Landsat data in estimating vegetation over can be problematic. Vegetation cover usually mixed with other land use / land cover components such as desertified land background, impervious surface, *etc*., within a pixel. In arid and semiarid regions, vegetation cover of low abundance represented by clump distributed natural desert shrubs, or of low biomass such as thin artificial grasslands for sand stabilization can be difficult to delineate at per-pixel level, owing to the spectral mixture and spectral confusion problems.

The recognition of the spectral mixture problem as well as attempts at sub-pixel analyses started in early 1970s, when the first earth resources satellite data were available (Blaschke, Lang, Lorup, Strobl, & Zeil, 2000; Nalepka & Hyde, 1972). Researches using Landsat 1 data brought out a major difficult called *mixed pixel problem*: the probability of correct classification can be significantly decreased when two or more types of vegetation occur within a given image element (Botkin, Estes, MacDonald, & Wilson, 1984). Over the past decades, studies have been conducted to solve the problem by unmixing pixels to determine the proportions of land cover components. A commonly used method is *spectral mixture analysis* (SMA) (Adams et al., 1995; Adams, Smith, & Johnson, 1986). SMA provides a solution to estimate the proportions of land cover fractions in a mixed pixel, which involves modeling a mixed spectrum as a combination of spectra for pure land cover types, referred to as endmembers (Adams et al., 1995; Wu & Murray, 2003) . Its simplest form is *linear spectral mixture model* (LSMM). The model takes the spectra of a pixel in each spectral band as a linear combination of the spectrum of its component endmembers weighted by their respective areal proportions within the pixel (Adams et al., 1995; Ichoku & Karnieli, 1996; Settle & Drake, 1993; Townshend et al., 2000). However, SMA depends on a number of user-defined parameters such as the number of endmembers and spectral signals of endmembers (Song, 2005). More importantly, the linearity assumption on SMA can be

easily violated due to the complexity of land cover composition and spatial structure at sub-pixel level. All these factors may lead to unsatisfactory sub-pixel mapping results.

In addition to SMA algorithm, there are other sub-pixel models using statistical approaches were developed for land cover composition, such as C-Means algorithm (Foody & Cox, 1994), pixel-swapping algorithm (Thornton, Atkinson, & Holland, 2006), maximum likelihood approach (Hung and Ridd 2002), *etc.* Recently, more studies have been employed advanced machine learning algorithms to obtain more accurate and more reliable land cover information at the sub-pixel level. The most commonly used machine learning algorithms comprise of Random Forest (RF) (Pal, 2005), Bagging (Prasad, Iverson, & Liaw, 2006), Boosting, Decision Tree, Supported Vector Machine (SVM) , Artificial Neural Network and K-Nearest-Neighbor (KNN) (Shao, Taff, & Walsh, 2011). With sufficient training data sets and appropriate parameters, these algorithms automatically generate the best model for the data using decision rules created from input data. Overall, these machine learning methods are non-parametric since they do not rely on any assumption about data distribution (Breiman, 2001) , and are designed to produce more accurate classification (Akar & Güngör, 2013).

The RF is a relative new machine learning algorithm. It is an ensemble classifier/regressor that can be described as a collection of decision tree classifiers/regressors. It is based on a basic premise that a set of classifiers perform better classifications than an individual classifier does, the RF uses same base classifier to produce repeated multiple classifications of the same data (Breiman, 2001; Rodriguez-Galiano, Ghimire, Rogan, Chica-Olmo, & Rigol-Sanchez, 2012). In training phase of RF, each classifier is generated using a random selected subset independently from the input variables; and in its classification phase, each tree casts a unit vote for the most popular class to classify an input variable. The output of

the classifier is determined by a majority vote of the trees (Breiman, 1999, 2001). Recently, RF is receiving highlighted interest in remote sensing community, and has been increasingly applied in LULC classification using satellite data (Chan & Paelinckx, 2008; Gislason, Benediktsson, & Sveinsson, 2006; Pal, 2005; Rodriguez-Galiano et al., 2012; Walton, 2008).

1.4 Image normalization

Image correction is a key preprocessing procedure in the development of methods for time-series inter-comparison or generalization of classifiers (Furby & Campbell, 2001; Song, Woodcock, Seto, Pax-Lenney, & Macomber, 2001). Although Landsat data have been preprocessed through radiometric and systematic geometric correction routines while employing DEM for topographic accuracy by USGS(USGS, 2012). However, there would be possible inconsistencies of radiometric measurements among multi-temporal imagery, due to potential variations in solar illumination conditions, atmospheric scattering and absorption, vegetation phenology variance, *etc.* (Schott, Salvaggio, & Volchok, 1988; Xian, Homer, & Fry, 2009). A number of radiometric normalization procedures have been developed to calibrate time-series data to common reference values. These procedures "optimize (Coppin & Bauer, 1994) " the data through transform of sensor data (*relative normalization*), or removal of exogenous image effects (*absolute normalization*), or a combination of the two. Relative normalization methods apply pairwise radiometric matching based on entire or partial information of the images. For example, the histogram matching using pseudo-invariant features (Collins & Woodcock, 1996; Furby & Campbell, 2001), and scene-to-scene linear histogram transformation (Schott, Salvaggio, and Volchok 1988; Xian, Homer, and Fry 2009; Yang, Xian, *et al.* 2003). Common absolute normalization methods include full image correction using radiative transfer codes (Gemmell, Varjo, & Strandstrom, 2001), and empirical image calibration using dense dark

vegetation approaches (Liang et al., 1997), dark object subtraction (DOS) approaches (Chavez, 1988), and so on. In addition, some studies applied relative normalization for atmospherically corrected data, these combined approaches have certain advantages (Coppin & Bauer, 1994) or limited improvement (Gemmell et al., 2001) over the use of single method alone.

DOS techniques take the spectral characteristics of the dark object as image noise to adjust radiance value for atmospheric degradation. The signal level of the dark noise for each image was subtracted from the image that it belongs, so as to put all images on a same radiometric scale (Chavez, 1988, 1996). There are some advantages of DOS. Firstly, comparing to other absolute normalization methods, DOS does not require *in situ* measurements during image acquisition which are needed for absolute full radiometric correction; Secondly, DOS has proved to be viable and efficient, while produces result with comparable accuracies as result from the more complex radiometric corrections for either image classification (Pax-Lenney, Woodcock, Macomber, Gopal, & Song, 2001) or change detection (Collins & Woodcock, 1996) purposes; Thirdly, the success of classification generalization and change detection procedures depend on an equivalence of radiometric measurement levels among time-series, rather than correction to standard reflectance units for each image (Schmidt, Jenkerson, Masek,, Vermote,, & Gao, 2013; Song et al., 2001)

Song (2001) summarized four specific DOS approaches (DOS1, DOS2, DOS3, and DOS4) involving different assumptions of atmospheric transmittance and diffuse irradiance. Generally, the model to convert at-satellite radiance (L_{sat}) to surface reflectance (ρ) by correcting solar and atmospheric effects is (Moran, Jackson, Slater, & Teillet, 1992; Song et al., 2001):

$$\rho = \frac{\pi(L_{sat} - L_p)}{T_v(E_0 cos(\theta_z) T_z + E_{down})} \quad (1)$$

where L_p is the path radiance, T_v is the atmospheric transmittance from the target toward the

sensor, T_z is the atmospheric transmittance in the illumination direction, E_0 is the exoatmospheric solar constant, and E_{down} is the downwelling spectral irradiance at the surface due to scattered solar flux in the atmosphere. In DOS1 approach, the loss of atmospheric transmittance and downwelling diffuse irradiance are ignored (*e.g.*, $T_v = 1$, $T_z = 1$, $E_{down} = 0$). According to Chavez (Chavez, 1996), 1% minimum reflectance for the dark object is suggested in consideration of the potential atmospheric scattering effect. The path radiance is given by (Sobrino, Jiménez-Muñoz, & Paolini, 2004):

$$L_p = L_{min} - L_{1\%} \quad (2)$$

where L_{min} is the radiance corresponds to a minimum digital count (DN) value derives from the satellite image, $L_{1\%}$ is the radiance of dark object, assumed to have a reflectance value of 0.01. Therefore, for Landsat 5 TM data (Song et al., 2001):

$$L_p = G \cdot DN_{min} + B - 0.01[E_0 \cos(\theta_z) T_z + E_{down}] T_v / \pi \quad (3)$$

where gain (G) and bias (B) are revised calibration parameters for Landsat 5 TM sensor, referring to Chander, *et. al* (Chander, Markham, & Barsi, 2007). DN_{min} is the minimum DN value with at least 1000 pixels. DOS1 assumes no atmospheric transmittance loss and diffuse downward at the surface, and is thus given by

$$\rho = \frac{\pi(L_{sat} - L_p)}{(E_0 \cos(\theta_z))} \quad (4)$$

1.5 Problem statement

In a context of long-term desertification and revegetation processes, oasis cities in the northwest China experienced intensive land use history accompanying significant urban expansion. All these processes are associated with vegetation cover dynamics. It is known the presence and dynamics of vegetation covers serve critical function in maintaining ecological balance, and are often closely related to the environmental security and sustainable urban

development. Their accurate mapping and assessment is thereby important for desertification monitoring, ecological management policy, and urban planning strategy. In this study, we focus on vegetation cover changes aiming to address three research questions:

(1) Whether integrated land use / land cover processes: revegetation and urbanization, brought about significant vegetation cover changes in oasis city in recent decades?

(2) If so, what are the spatial and temporal patterns of such vegetation dynamics?

For exploring these questions, we take Zhongwei City as an intensive study area to quantify the urbanization and revegetation processes through a unified sub-pixel measure of vegetation cover. We develop our remote sensing mapping and vegetation change detection techniques with RF algorithm and DOS1 image normalization technique. Vegetation dynamics are characterized using multiple Landsat images from different years (1990-2011). Specific research strategies included the following:

(1) Conduct sub-pixel vegetation mapping by integrating high (OrbView-3) and medium spatial resolution (Landsat) data,

(2) Examine simple atmospheric correction method to support temporal generalization of sub-pixel mapping algorithm,

(3) And characterize patterns of vegetation cover dynamics based on change detection analysis.

These three strategies presented in this study are potentially important to researchers attempting to monitor urban landscape dynamics in the arid and semiarid region of northwest China. Details of methodology and results are presented in Chapter 2.

References

Adams, J. B., Sabol, D. E., Kapos, V., Almeida Filho, R., Roberts, D. A., Smith, M. O., & Gillespie, A. R. (1995). Classification of multispectral images based on fractions of endmembers: Application to land-cover change in the Brazilian Amazon. *Remote Sensing of Environment*, *52*(2), 137–154. doi:10.1016/0034-4257(94)00098-8

Adams, J. B., Smith, M. O., & Johnson, P. E. (1986). Spectral mixture modeling: A new analysis of rock and soil types at the Viking Lander 1 Site. *Journal of Geophysical Research: Solid Earth*, *91*(B8), 8098–8112. doi:10.1029/JB091iB08p08098

Akar, Ö., & Güngör, O. (2013). Classification of multispectral images using Random Forest algorithm. *Journal of Geodesy and Geoinformation*, *1*(2), 105–112.

Blaschke, T., Lang, S., Lorup, E., Strobl, J., & Zeil, P. (2000). Object-oriented image processing in an integrated GIS/remote sensing environment and perspectives for environmental applications. *Environmental Information for Planning, Politics and the Public*, *2*, 555–570.

Botkin, D. B., Estes, J. E., MacDonald, R. M., & Wilson, M. V. (1984). Studying the Earth's Vegetation from Space. *BioScience*, *34*(8), 508–514. doi:10.2307/1309693

Bovolo, F., Bruzzone, L., & Carlin, L. (2010). A Novel Technique for Subpixel Image Classification Based on Support Vector Machine. *Image Processing, IEEE Transactions on*, *19*(11), 2983–2999. doi:10.1109/TIP.2010.2051632

Brazel, A., Selover, N., Vose, R., & Heisler, G. (2000). The tale of two climates-Baltimore and Phoenix urban LTER sites. *Climate Research*, *15*(2), 123–135.

Breiman, L. (1999). *Random forests-random features* (No. Technical Report 567). Berkeley, CA: Department of Statistics, University of California.

Breiman, L. (2001). Random Forests. *Machine Learning*, *45*(1), 5–32. doi:10.1023/A:1010933404324

Cao, S. (2008). Why Large-Scale Afforestation Efforts in China Have Failed To Solve the Desertification Problem. *Environmental Science & Technology*, *42*(6), 1826–1831. doi:10.1021/es0870597

Chan, J. C.-W., & Paelinckx, D. (2008). Evaluation of Random Forest and Adaboost tree-based ensemble classification and spectral band selection for ecotope mapping using airborne hyperspectral imagery. *Remote Sensing of Environment*, *112*(6), 2999–3011. doi:10.1016/j.rse.2008.02.011

Chander, G., Markham, B. L., & Barsi, J. A. (2007). Revised Landsat-5 thematic mapper radiometric calibration. *Geoscience and Remote Sensing Letters, IEEE*, *4*(3), 490–494.

Chavez, P. S. (1988). An improved dark-object subtraction technique for atmospheric scattering correction of multispectral data. *Remote Sensing of Environment*, *24*(3), 459–479. doi:10.1016/0034-4257(88)90019-3

Chavez, P. S. (1996). Image-based atmospheric corrections-revisited and improved. *Photogrammetric Engineering and Remote Sensing*, *62*(9), 1025–1035.

Chen, Y., & Tang, H. (2005). Desertification in north China: background, anthropogenic impacts and failures in combating it. *Land Degradation & Development*, *16*(4), 367–376. doi:10.1002/ldr.667

Collins, J. B., & Woodcock, C. E. (1996). An assessment of several linear change detection techniques for mapping forest mortality using multitemporal landsat TM data. *Remote Sensing of Environment*, *56*(1), 66–77. doi:10.1016/0034-4257(95)00233-2

Coppin, P. R., & Bauer, M. E. (1994). Processing of multitemporal Landsat TM imagery to optimize extraction of forest cover change features. *Geoscience and Remote Sensing, IEEE Transactions on*, *32*(4), 918–927. doi:10.1109/36.298020

Cutler, D. R., Edwards Jr, T. C., Beard, K. H., Cutler, A., Hess, K. T., Gibson, J., & Lawler, J. J. (2007). Random forests for classification in ecology. *Ecology*, *88*(11), 2783–2792.

Elmore, A. J., Mustard, J. F., Manning, S. J., & Lobell, D. B. (2000). Quantifying Vegetation Change in Semiarid Environments: Precision and Accuracy of Spectral Mixture Analysis and the Normalized Difference Vegetation Index. *Remote Sensing of Environment*, *73*(1), 87–102. doi:10.1016/S0034-4257(00)00100-0

Feng, W., Fan, Xu., Lu, T., & Feng, W. (Eds.). (1998). *Zhongwei Yearbook 1994-1995* (Chinese Edition.). Yinchuan: Ningxia People's Publishing House.

Foody, G. M., & Cox, D. P. (1994). Sub-pixel land cover composition estimation using a linear mixture model and fuzzy membership functions. *International Journal of Remote Sensing*, *15*(3), 619–631. doi:10.1080/01431169408954100

Fullen, M. A., & Mitchell, D. J. (1994). Desertification and reclamation in north-central China. *Ambio*, 131–135.

Furby, S. L., & Campbell, N. A. (2001). Calibrating images from different dates to "like-value" digital counts. *Remote Sensing of Environment*, *77*(2), 186–196. doi:10.1016/S0034-4257(01)00205-X

Gemmell, F., Varjo, J., & Strandstrom, M. (2001). Estimating forest cover in a boreal forest test site using Thematic Mapper data from two dates. *Remote Sensing of Environment*, *77*(2), 197–211. doi:10.1016/S0034-4257(01)00206-1

Gislason, P. O., Benediktsson, J. A., & Sveinsson, J. R. (2006). Random Forests for land cover classification. *Pattern Recognition in Remote Sensing (PRRS 2004)*, *27*(4), 294–300. doi:10.1016/j.patrec.2005.08.011

Han, D., & Meng, X. (1999). Recent progress of research on Oasis in China. *Chinese Geographical Science*, *9*(3), 199–205. doi:10.1007/s11769-999-0044-x

Homer, C., Huang, C., Yang, L., Wylie, B. K., & Coan, M. (2004). Development of a 2001 national land-cover database for the United States.

Hung, M.-C., & Ridd, M. K. (2002). A subpixel classifier for urban land-cover mapping based on a maximum-likelihood approach and expert system rules. *Photogrammetric Engineering and Remote Sensing*, *68*(11), 1173–1180.

Ichoku, C., & Karnieli, A. (1996). A review of mixture modeling techniques for sub-pixel land cover estimation. *Remote Sensing Reviews*, *13*(3-4), 161–186. doi:10.1080/02757259609532303

Ji, M., & Jensen, J. R. (1999). Effectiveness of Subpixel Analysis in Detecting and Quantifying Urban Imperviousness from Landsat Thematic Mapper Imagery. *Geocarto International*, *14*(4), 33–41. doi:10.1080/10106049908542126

Jiang, L. (Ed.). (2004). *China Central Western Area Development Yearbook* (Chinese Edition.). Beijing: China Financial and Economic Publishing House. Retrieved from http://book.chaoxing.com/ebook/read_11377869.html

Liang, S., Fallah-Adl, H., Kalluri, S., JáJá, J., Kaufman, Y. J., & Townshend, J. R. G. (1997). An operational atmospheric correction algorithm for Landsat Thematic Mapper imagery over the land. *Journal of Geophysical Research: Atmospheres*, *102*(D14), 17173–17186. doi:10.1029/97JD00336

Lin, W., & Chen, T. P. (2004). China's widening economic disparities and its "Go West Program." *Journal of Contemporary China*, *13*(41), 663–686. doi:10.1080/1067056042000281422

Liu, Y. (2012). Analysis of Current Situation in Land Utilization in Shapotou District of Zhongwei Municipality. *Ningxia Journal of Agriculture and Forestry Science and Technology*, *53*(11), 129–130.

Lu, D., & Weng, Q. (2004). Spectral mixture analysis of the urban landscape in Indianapolis with Landsat ETM+ imagery. *Photogrammetric Engineering and Remote Sensing*, *70*(9), 1053–1062.

Lu, D., & Weng, Q. (2006). Use of impervious surface in urban land-use classification. *Remote Sensing of Environment*, *102*(1–2), 146–160. doi:10.1016/j.rse.2006.02.010

Ma, Q. (2004). Appraisal of Tree Planting Options to Control Desertification: Experiences from Three-North Shelterbelt Programme. *International Forestry Review*, *6*(3-4), 327–334. doi:10.1505/ifor.6.3.327.59972

Ma, Y., Fan, S., Zhou, L., Dong, Z., Zhang, K., & Feng, J. (2007). The temporal change of driving factors during the course of land desertification in arid region of North China: the case of Minqin County. *Environmental Geology*, *51*(6), 999–1008. doi:10.1007/s00254-006-0369-z

Masek, J. G., Vermote, E. F., Saleous, N. E., Wolfe, R., Hall, F. G., Huemmrich, K. F., … Lim, T.-K. (2006). A Landsat surface reflectance dataset for North America, 1990-2000. *Geoscience and Remote Sensing Letters, IEEE*, *3*(1), 68–72.

McDonald, A. . J., Gemmell, F. M., & Lewis, P. E. (1998). Investigation of the Utility of Spectral Vegetation Indices for Determining Information on Coniferous Forests. *Remote Sensing of Environment*, *66*(3), 250–272. doi:10.1016/S0034-4257(98)00057-1

McGwire, K., Minor, T., & Fenstermaker, L. (2000). Hyperspectral Mixture Modeling for Quantifying Sparse Vegetation Cover in Arid Environments. *Remote Sensing of Environment*, *72*(3), 360–374. doi:10.1016/S0034-4257(99)00112-1

Mitchell, D. J., Fullen, M. A., Trueman, I. C., & Fearnehough, W. (1998). Sustainability of reclaimed desertified land in Ningxia, China. *Journal of Arid Environments*, *39*(2), 239–251. doi:10.1006/jare.1998.0396

Moran, M. S., Jackson, R. D., Slater, P. N., & Teillet, P. M. (1992). Evaluation of simplified procedures for retrieval of land surface reflectance factors from satellite sensor output. *Remote Sensing of Environment*, *41*(2–3), 169–184. doi:10.1016/0034-4257(92)90076-V

Nalepka, R. F., & Hyde, P. D. (1972). Classifying unresolved objects from simulated space data. In *Proceedings of the Eighth International Symposium on Remote Sensing of Environment* (Vol. 2, pp. 935–949). Environmental Research Institute of Michigan,Ann Arbor, Michigan. Retrieved from http://ntrs.nasa.gov/search.jsp?R=19730055080

Nicholson, S. E., Tucker, C. J., & Ba, M. B. (1998). Desertification, Drought, and Surface Vegetation: An Example from the West African Sahel. *Bulletin of the American Meteorological Society*, *79*(5), 815–829. doi:10.1175/1520-0477(1998)079<0815:DDASVA>2.0.CO;2

Orbital Imaging Corporation. (2006). *OrbView-3: Fact sheet*. Dulles, VA: Orbital Sciences Corporation. Retrieved from http://www.orbital.com/newsinfo/publications/ov3_fact.pdf

Pal, M. (2005). Random forest classifier for remote sensing classification. *International Journal of Remote Sensing*, *26*(1), 217–222. doi:10.1080/01431160412331269698

Pax-Lenney, M., Woodcock, C. E., Macomber, S. A., Gopal, S., & Song, C. (2001). Forest mapping with a generalized classifier and Landsat TM data. *Remote Sensing of Environment*, *77*(3), 241–250. doi:10.1016/S0034-4257(01)00208-5

Phinn, S., Stanford, M., Scarth, P., Murray, A. T., & Shyy, P. T. (2002). Monitoring the composition of urban environments based on the vegetation-impervious surface-soil (VIS)

model by subpixel analysis techniques. *International Journal of Remote Sensing*, *23*(20), 4131–4153. doi:10.1080/01431160110114998

Powell, R. L., Roberts, D. A., Dennison, P. E., & Hess, L. L. (2007). Sub-pixel mapping of urban land cover using multiple endmember spectral mixture analysis: Manaus, Brazil. *Remote Sensing of Environment*, *106*(2), 253–267. doi:10.1016/j.rse.2006.09.005

Prasad, A. M., Iverson, L. R., & Liaw, A. (2006). Newer Classification and Regression Tree Techniques: Bagging and Random Forests for Ecological Prediction. *Ecosystems*, *9*(2), 181–199. doi:10.1007/s10021-005-0054-1

Qi, S. Z., Li, X. Y., & Duan, H. P. (2007). Oasis land-use change and its environmental impact in Jinta Oasis, arid northwestern China. *Environmental Monitoring and Assessment*, *134*(1-3), 313–320. doi:10.1007/s10661-007-9622-5

Rashed, T., & Jürgens, C. (Eds.). (2010). *Remote sensing of urban and suburban areas*. Dordrecht ; London: Springer.

Ridd, M. K. (1995). Exploring a V-I-S (vegetation-impervious surface-soil) model for urban ecosystem analysis through remote sensing: comparative anatomy for cities. *International Journal of Remote Sensing*, *16*(12), 2165–2185. doi:10.1080/01431169508954549

Rodriguez-Galiano, V. F., Ghimire, B., Rogan, J., Chica-Olmo, M., & Rigol-Sanchez, J. P. (2012). An assessment of the effectiveness of a random forest classifier for land-cover classification. *ISPRS Journal of Photogrammetry and Remote Sensing*, *67*(0), 93–104. doi:10.1016/j.isprsjprs.2011.11.002

Schmidt, G., Jenkerson, C., Masek,, J., Vermote,, E., & Gao, F. (2013). *Landsat Ecosystem Disturbance Adaptive Processing System (LEDAPS) Algorithm Description* (No. Open-File Report 2013–1057) (p. 27). Reston, Virginia: U.S. Geological Survey. Retrieved from http://pubs.usgs.gov/of/2013/1057/ofr13_1057.pdf

Schneider, A., Seto, K. C., & Webster, D. R. (2005). Urban growth in Chengdu, Western China: application of remote sensing to assess planning and policy outcomes. *Environment and Planning B: Planning and Design*, *32*(3), 323–345.

Schott, J. R., Salvaggio, C., & Volchok, W. J. (1988). Radiometric scene normalization using pseudoinvariant features. *Remote Sensing of Environment*, *26*(1), 1–16. doi:10.1016/0034-4257(88)90116-2

Settle, J. J., & Drake, N. A. (1993). Linear mixing and the estimation of ground cover proportions. *International Journal of Remote Sensing*, *14*(6), 1159–1177. doi:10.1080/01431169308904402

Shalaby, A., Ghar, M. A., & Tateishi, R. (2004). Desertification impact assessment in Egypt using low resolution satellite data and GIS. *International Journal of Environmental Studies*, *61*(4), 375–383. doi:10.1080/0020723042000199740

Shalaby, A., & Tateishi, R. (2007). Remote sensing and GIS for mapping and monitoring land cover and land-use changes in the Northwestern coastal zone of Egypt. *Applied Geography*, *27*(1), 28–41. doi:10.1016/j.apgeog.2006.09.004

Shao, X. (2011). *Study on artificial forest dynamics using object-based image analysis at Shapotou District, Zhongwei City, Ningxia Autonomous Region* (Master Thesis). Lanzhou University, Lanzhou, China. Retrieved from http://cdmd.cnki.com.cn/Article/CDMD-10730-1012373169.htm

Shao, Y., & Lunetta, R. S. (2012). Comparison of support vector machine, neural network, and CART algorithms for the land-cover classification using limited training data points. *ISPRS Journal of Photogrammetry and Remote Sensing*, *70*(0), 78–87. doi:10.1016/j.isprsjprs.2012.04.001

Shi, P.-J., Shimizu, H., Wang, J.-A., Liu, L.-Y., Li, X.-Y., Fan, Y.-D., … Song, Y. (2005). Land degradation and blown-sand disaster in China. In K. Omasa, I. Nouchi, & L. Kok (Eds.), *Plant Responses to Air Pollution and Global Change* (pp. 261–269). Tokyo: Springer Japan. Retrieved from http://dx.doi.org/10.1007/4-431-31014-2_29

Small, C. (2001). Estimation of urban vegetation abundance by spectral mixture analysis. *International Journal of Remote Sensing*, *22*(7), 1305–1334. doi:10.1080/01431160151144369

Smith, M. O., Ustin, S. L., Adams, J. B., & Gillespie, A. R. (1990). Vegetation in deserts: II. Environmental influences on regional abundance. *Remote Sensing of Environment*, *31*(1), 27–52. doi:10.1016/0034-4257(90)90075-W

Sobrino, J. A., Jiménez-Muñoz, J. C., & Paolini, L. (2004). Land surface temperature retrieval from LANDSAT TM 5. *Remote Sensing of Environment*, *90*(4), 434–440. doi:10.1016/j.rse.2004.02.003

Song, C. (2005). Spectral mixture analysis for subpixel vegetation fractions in the urban environment: How to incorporate endmember variability? *Remote Sensing of Environment*, *95*(2), 248–263. doi:10.1016/j.rse.2005.01.002

Song, C., Woodcock, C. E., Seto, K. C., Pax-Lenney, M., & Macomber, S. A. (2001). Classification and Change Detection Using Landsat TM Data: When and How to Correct Atmospheric Effects? *Remote Sensing of Environment*, *75*(2), 230–244. doi:10.1016/S0034-4257(00)00169-3

State Forestry Administration, P. R. China. (2011). *A Bulletin of Status Quo of Desertification and Sandification in China*.

Statistical Bureau of Ningxia Hui Autonomous Region, & Survey Office of the National Bureau of Statistics in Ningxia Hui Autonomous Region (Eds.). (2012). *Ningxia Statistical Yearbook*. Beijing, China: China Statistics Press.

Su, Y. Z., Zhao, W. Z., Su, P. X., Zhang, Z. H., Wang, T., & Ram, R. (2007). Ecological effects of desertification control and desertified land reclamation in an oasis–desert ecotone in an arid region: A case study in Hexi Corridor, northwest China. *Ecological Engineering*, *29*(2), 117–124. doi:10.1016/j.ecoleng.2005.10.015

Teillet, P. M., & Fedosejevs, G. (1995). On the dark target approach to atmospheric correction of remotely sensed data. *Canadian Journal of Remote Sensing*, *21*(4), 374–387.

Thornton, M. W., Atkinson, P. M., & Holland, D. A. (2006). Sub-pixel mapping of rural land cover objects from fine spatial resolution satellite sensor imagery using super-resolution pixel-swapping. *International Journal of Remote Sensing*, *27*(3), 473–491. doi:10.1080/01431160500207088

Tooke, T. R., Coops, N. C., Goodwin, N. R., & Voogt, J. A. (2009). Extracting urban vegetation characteristics using spectral mixture analysis and decision tree classifications. *Remote Sensing of Environment*, *113*(2), 398–407. doi:10.1016/j.rse.2008.10.005

Townshend, J. R. G., Huang, C., Kalluri, S. N. V., Defries, R. S., Liang, S., & Yang, K. (2000). Beware of per-pixel characterization of land cover. *International Journal of Remote Sensing*, *21*(4), 839–843. doi:10.1080/014311600210641

UNDP. (n.d.). Ningxia Anti-desertification and Livelihood Improvement. Retrieved September 18, 2013, from http://www.undp.org/content/china/en/home/operations/projects/environment_and_energy/ningxia-anti-desertification-and-livelihood-improvement-/

USGS. (2012, January 24). OrbView-3. *USGS Long Term Archive*. U.S. Geological Survey. Retrieved January 11, 2014, from https://lta.cr.usgs.gov/satellite_orbview3

Walton, J. T. (2008). Subpixel urban land cover estimation: comparing cubist, random forests, and support vector regression. *Photogrammetric Engineering and Remote Sensing*, *74*(10), 1213–1222.

Wang, S., Ma, Y., Hou, Q., & Wang, Y. (2007). Coping Strategies with Desertification in China. In M. V. K. Sivakumar & R. P. Motha (Eds.), *Managing Weather and Climate Risks in Agriculture* (pp. 317–341). Springer Berlin Heidelberg. Retrieved from http://dx.doi.org/10.1007/978-3-540-72746-0_18

Wang, T., Wu, W., Xue, X., Sun, Q., & Chen, G. (2004). Study of spatial distribution of sandy desertification in North China in recent 10 years. *Science in China Series D: Earth Sciences*, *47*(1), 78–88. doi:10.1360/04zd0009

Wang, X. M., Zhang, C. X., Hasi, E., & Dong, Z. B. (2010). Has the Three Norths Forest Shelterbelt Program solved the desertification and dust storm problems in arid and semiarid China? *Journal of Arid Environments*, *74*(1), 13–22. doi:10.1016/j.jaridenv.2009.08.001

Wu, C., & Murray, A. T. (2003). Estimating impervious surface distribution by spectral mixture analysis. *Remote Sensing of Environment*, *84*(4), 493–505. doi:10.1016/S0034-4257(02)00136-0

Wu, H. (Ed.). (2011). *Zhongwei Yearbook 2010* (Chinese Edition.). Yinchuan: Ningxia People's Publishing House.

Wu, H. (Ed.). (2013). *Zhongwei Yearbook 2012* (Chinese Edition.). Yinchuan: Ningxia People's Publishing House.

Xian, G., Homer, C., & Fry, J. (2009). Updating the 2001 National Land Cover Database land cover classification to 2006 by using Landsat imagery change detection methods. *Remote Sensing of Environment*, *113*(6), 1133–1147. doi:10.1016/j.rse.2009.02.004

Yan, C., Wang, Y., Feng, Y., & Wang, J. (2003). Macro-scale Survey and Dynamic Studies of Sandy Land in Ningxia by Remote Sensing. *Journal of Desert Reserch*, *23*(2), 132–135.

Yang, L., Huang, C., Homer, C. G., Wylie, B. K., & Coan, M. J. (2003). An approach for mapping large-area impervious surfaces: synergistic use of Landsat-7 ETM+ and high spatial resolution imagery. *Canadian Journal of Remote Sensing*, *29*(2), 230–240. doi:10.5589/m02-098

Yang, L., Lan, Z., & Wu, J. (2010). Roles of Scholars in the Practice of Combating-Desertification: A Case Study in Northwest China. *Environmental Management*, *46*(2), 154–166. doi:10.1007/s00267-010-9534-y

Yang, L., Xian, G., Klaver, J. M., & Deal, B. (2003). Urban land-cover change detection through sub-pixel imperviousness mapping using remotely sensed data. *Photogrammetric Engineering and Remote Sensing*, *69*(9), 1003–1010.

Yang S., Taff, G. N., & Walsh, S. J. (2011). Comparison of Early Stopping Criteria for Neural-Network-Based Subpixel Classification. *Geoscience and Remote Sensing Letters, IEEE*, *8*(1), 113–117. doi:10.1109/LGRS.2010.2052782

Zhu, Z. (1989). Advance in Desertification Research in China. *Journal of Desert Research*, *1*.

Chapter 2: Monitoring Vegetation Dynamics in Zhongwei, an Arid City of Northwest China

2.1 Introduction

The deserts and desertified lands of China cover 2,623,700 km^2, about 27.33% of total area of China (State Forestry Administration, P. R. China, 2011). Most of China's deserts are located in the north and northwest regions and many are expanding in a southerly direction (Mitchell, Fullen, Trueman, & Fearnehough, 1998; State Forestry Administration, P. R. China, 2011). At the national scale, estimated annual desertification rates increased from 1,560 km^2 in 1970s to 3,600 km^2 in late 1990s (Wang et al., 2004). Desertification-prone areas include grassland, pasture lands, and oasis croplands at the periphery of deserts (Su et al., 2007; Wang et al., 2004). The drivers of desertification include both climatic forces (*e.g.*, droughts) and human-driven factors such as overgrazing, irrational use of water resources, and population growth. In recent studies human-driven factors appeared to be more important than natural factors in desertification processes in arid areas of northern China (Chen & Tang, 2005; Ma et al., 2007).

The environmental and socio-economic impacts of desertification are well recognized (Fullen and Mitchell 1994; Chen and Tang 2005; Wang *et al.* 2007; Yang, *et al.* 2010). The Chinese Central Government has implemented several national afforestation and desert reclamation programs to increase forest coverage and combat desertification, sand encroachment, and dust storms (Wang et al., 2010; Zhu, 1989). For example, the Three North Shelter Forest System Project (started in 1978) which is one of the most ambitious afforestation program, plans to build a 2800-mile long tree belt to control the expansion of the Gobi Desert (Cao, 2008; Lin & Chen, 2004). Extensive regional and local revegetation programs have also been implemented. Many of these programs focused on building tree/vegetation belt to control the expansion of

deserts and fix sand dunes, and it is not uncommon to see reclamation of desert lands through the expansion of woody vegetation (Cao, 2008).

In the context of desertification and afforestation processes, oases (isolated areas of vegetation) of arid northwestern China have received much attention due to their economic and ecological importance. While they only cover a small portion (<3%) of land surface area, oases support over 95% of the region's population and account for 90% of gross domestic product (Han & Meng, 1999; Su et al., 2007). Ecologically, oases are considered fragile ecosystems because of their close proximity to desert, limited spatial extents, and intensive land use histories (*e.g.*, overgrazing) (Qi, Li, & Duan, 2007). Recently, urbanization of oases in arid northwest China is also increasing. Urban expansion in these areas is partially stimulated by China's 'Go West' program that promotes development of central and western China in order to reduce inland–coastal inequality (Lin & Chen, 2004). One key component of the 'Go West' program is prioritization of central city/town development in western China with the aim of using those cities as an engine to generate regional growth (Schneider et al., 2005). Few published studies have quantified the rates of urban expansion for oasis cities in the northwest China, but some researchers have raised questions on potential negative environmental consequences such as land/vegetation degradation, decline of ground water, and overall ecosystem services (Qi et al., 2007).

Urban expansion, desertification, and revegetation processes in oases combine to generate complex land use and land cover patterns and change trajectories that provide a challenging but intriguing setting in which to study human-environment interactions in arid regions (Shalaby et al., 2004). All three processes are associated with vegetation cover dynamics. Urban expansion includes the conversion of natural vegetation, or agricultural lands, to

impervious surface (Ridd, 1995). Although the nature and character of desertification remain controversial, an increasing number of studies have used vegetation information, especially remote sensing-based vegetation indices (*e.g.*, the Normalized Difference Vegetation Index or NDVI), as a systematic measure of desertification processes (Nicholson, Tucker, & Ba, 1998). The revegetation program in China mainly involves tree-planting, which would increase vegetation cover initially. The spatial-temporal variability of vegetation cover, derived from remote sensing data, can provide a valuable index to monitor all three land cover change processes and provide insights on the relationships between land cover changes and associated surface biophysical processes (Lu & Weng, 2004; Phinn, Stanford, Scarth, Murray, & Shyy, 2002; Ridd, 1995; Tooke, Coops, Goodwin, & Voogt, 2009).

To date, few researchers have used remote sensing data to monitor and assess vegetation dynamics of oasis city in the arid/semiarid northwest China. Most oasis studies have focused on ecosystem restoration, ecological engineering, or plant physiology (*e.g.*, Yan *et al.* 2003; Shao 2011; Liu 2012). Quantitative measures of afforestation or revegetation programs are rarely reported and results can be controversial (Cao, 2008; Ma, 2004). Urban expansion in arid northwest China has not been thoroughly examined; most studies of urbanization in China favor mega-cities such as Beijing, Shanghai, and Guangzhou in the coastal region (Schneider et al., 2005). Desertification, revegetation, and urban expansion processes and their interactions should be examined simultaneously to provide an overall picture of landscape dynamics and their linked ecosystem functions.

The overall goal of this study is to document vegetation dynamics in Zhongwei City, northwest China across two decades using remote sensing mapping and change detection techniques and link changes with processes of urbanization and revegetation. Zhongwei is an

oasis city located in Ningxia Hui Autonomous Region. Desertification has been notorious in Zhongwei since early 1950s (Yang, Lan, and Wu 2010). To protect the Yellow River and the 40 km of railway from sand storm encroachment, the central and local governments has developed revegetation programs to combat desertification in Zhongwei (*e.g.*, Wang *et al.* 2007; Yang, Lan, and Wu 2010, Feng *et al.* 1998; UNDP 2013). Zhongwei city is representative of small and medium-sized cities in the arid region of northwest China where desertification, revegetation, and urban expansion processes interact to shape landscape patterns and functions.

The two objectives of this study is to use Zhongwei City to develop remote sensing mapping and vegetation change detection techniques; And to document recent vegetation cover dynamics, and link changes with the processes of urbanization and revegetation.

In this study, we quantify the urbanization and revegetation processes through a unified sub-pixel measure of vegetation cover. Vegetation dynamics are characterized using multiple Landsat images from different years (1990-2011). Specific research strategies included the following:

(1) conduct sub-pixel vegetation mapping by integrating high (OrbView-3) and medium spatial resolution (Landsat) data,

(2) examine simple atmospheric correction method to support temporal generalization of sub-pixel mapping algorithm, and

(3) characterize patterns of vegetation cover dynamics based on change detection analysis.

These three strategies are potentially important to researchers attempting to monitor landscape dynamics in the arid region of northwest China.

2.2 Background on sub-pixel vegetation mapping

Remote sensing-based urban vegetation mapping has a long history, particularly using medium spatial resolution data such as those from Landsat series of sensors (Ridd, 1995; Small, 2001; Song, 2005; Wu & Murray, 2003). The conceptual Vegetation - Impervious surface- Soil (V-I-S) model has been intensively used to characterize urban landscape and vegetation cover is a key component to address questions of urban morphology, spatial structure, and spatial-temporal dynamics (Lu & Weng, 2004; Phinn et al., 2002; Ridd, 1995; Tooke et al., 2009) .

Vegetation mapping in urban/suburban areas is challenging because vegetation surfaces are often mixed with other land covers (*e.g.*, impervious surfaces), particularly when observed at medium spatial resolution (*e.g.*, Landsat, 30-m) remote sensing data (Ridd, 1995; Song, 2005). Spectral mixtures and spectral confusion impose significant difficulties for robust mapping of vegetation surfaces(McGwire, Minor, & Fenstermaker, 2000). Similarly, in arid and semiarid environments, vegetation cover is sparse and spectral signals from vegetation are confounded by strong background surfaces (*e.g.*, soil, sand). The use of traditional per-pixel classification techniques can be problematic, because large numbers of pixels may have mixed spectral signals from two or more land cover types. With medium spatial resolution Landsat imagery as primary input data, many researchers have applied linear spectral mixture analysis (SMA) to estimate sub-pixel vegetation fraction for urban (Phinn et al., 2002; Powell, Roberts, Dennison, & Hess, 2007) and arid desert regions (Elmore, Mustard, Manning, & Lobell, 2000; Smith, Ustin, Adams, & Gillespie, 1990). The fundamental assumption of SMA is that spectral signal for a mixed pixel is a linear combination of spectra from endmembers, or pure land cover types (Adams et al., 1995; Wu & Murray, 2003). The most commonly used endmembers include vegetation, impervious surface, and soil (Ridd 1995) for urban setting. Impervious surface may be further divided into high- and low-albedo impervious endmembers (Wu & Murray, 2003). The main

advantage of SMA is that it is a physical-based solution and conceptually simple. However, the performance of SMA mapping is depending on a number of user-defined parameters such as the number of endmembers and spectral signals of endmembers (Song, 2005), more importantly, the linearity assumption on SMA can be easily violated due to the complexity of land cover composition and spatial structure at sub-pixel level. All these factors may lead to unsatisfactory sub-pixel mapping results.

In additional to the SMA algorithm, many statistical approaches for sub-pixel mapping have been developed, including Fuzzy c-Means algorithm (Foody & Cox, 1994), pixel-swapping algorithm (Thornton et al., 2006), and maximum likelihood approach (Hung & Ridd, 2002). More recently, machine learning algorithms have become increasingly popular in sub-pixel mapping. The most commonly used machine learning algorithms include Artificial Neural Network (Shao et al., 2011), regression trees (Yang, Huang, Homer, Wylie, & Coan, 2003), Random Forest (RF) (Pal, 2005), Supported Vector Machine (SVM) (Bovolo, Bruzzone, & Carlin, 2010). For example, the 30-m resolution percent tree canopy map, a part of the National Land Cover Database 2001 (NLCD 2001) product, was developed using a regression tree algorithm (Homer, Huang, Yang, Wylie, & Coan, 2004). A large number of high resolution aerial photos (*e.g.*, 1-m National Agriculture Imagery Program imagery) were processed first to derive two-class (*i.e.*, tree canopy or non-canopy) map products. These fine resolution tree canopy map products were rescaled to 30-m spatial resolution to provide percent tree canopy, a main training dataset for sub-pixel tree canopy mapping using medium spatial resolution Landsat data. Similar analytical approach will be used for percent tree canopy mapping of NLCD 2011, and RF will be used as the primary algorithm. RF algorithm is an extension of Classification and Regression Tree (CART). It is one of ensemble classifiers that grow large number of trees (*e.g.*,

500-2000) and average all trees to derive the final prediction (Breiman, 2001). By combining results from large number of trees, RFs achieve both low bias and low variance, and obtain high prediction accuracy for new data sets (Breiman, 2001; Cutler et al., 2007; Prasad et al., 2006; Rodriguez-Galiano et al., 2012). It should be noted that each mapping algorithm has its own advantages and drawbacks. With sufficient training data points and appropriate parameter-adjusting, almost all of these advanced machine learning algorithms perform well for the remote sensing mapping purpose (Shao & Lunetta, 2012).

2.3 Methods

2.3.1 Study area

Zhongwei city (104.28 º– 105.62 ºE, 36.98 º– 37.72 ºN) is located in Ningxia Hui Autonomous Region (Ningxia), northwestern China (Figure 1). The city lies at the edge of an oasis and abuts the southeastern frontier of the Tengger Desert, the fourth largest desert in China. The Yellow River traverses the irrigated plain of the city and provides critical water source for agriculture production. Zhongwei was a linchpin of the Silk Road in ancient times. Now it is a hub of national transportation networks. For example, Lanzhou–Baotou Railway, the nation's first desert railway, passes through the city (Feng et al., 1998; Wu, 2013). Zhongwei covers a total area of 16,986 km^2. Over 90% of areas are mountains, loess hilly region, and desert (Wu, 2013). Centuries of overgrazing and forest destruction caused severe land degradation in this area. In recent decades, many rehabilitation projects have been implemented in the periphery of city to restrain ecological degradation (Feng et al., 1998; Jiang, 2004; UNDP, n.d.; Wang et al., 2007).

Our study focused on the city municipal district. During our study period, the population of Zhongwei increased from 289,527 to 335,374 between 1990 and 2000 and to 383,014 by 2012

(Statistical Bureau of Ningxia Hui Autonomous Region & Survey Office of the National Bureau of Statistics in Ningxia Hui Autonomous Region, 2012). Zhongwei, as a desert oasis, is now also a popular tourism destination and draws over 2 million tourists every year. The tourism industry generates economic benefits for the area, but environmental impacts associated travel, accommodation, and recreational activities also need to be assessed to support sustainability.

2.3.2 Data

Four Landsat 5 TM images (1990, 1996, 2004 and 2011; path 130, row 34) were obtained from the United States Geological Survey (USGS) Landsat Earth Resources Observation Systems (EROS) Data Center (Table 1). These images were acquired 6-8 years apart over the 22-year period. We selected near-anniversary (August) images to minimize phenological variations and all images are cloud free. Other cloud-free images from late spring and early summer were also considered, but a substantial proportion of agricultural fields was in the flooding and rice transplanting period, thus not ideal for vegetation mapping. For each Landsat scene, we created an image subset (1,036 km^2) to cover the urban core and its surrounding deserts (Figure 2). All the images were registered to the 2004 master image through image-to-image registration.

We obtained two high spatial resolution OrbView-3 satellite images (by Orbital Imaging Corporation, now GeoEye, Inc.) from the USGS EROS Date Center (Table 2). One OrbView-3 multispectral image was acquired on June 20, 2004, at 4-m spatial resolution. It has four spectral bands (visible and infrared) that are of comparable spectral resolution as Landsat imagery (Orbital Imaging Corporation, 2006). The other panchromatic image was acquired on March 4, 2004 at 1-meter spatial resolution. The spatial extents of the multispectral and panchromatic images are about 8km x 25km and about 8km x 35km, respectively. The coverages of two

images run through Zhongwei city from north to south and have overlap at the urban core area (Figure 3). Both images are of high quality and cloud-free.

2.3.3 Images preprocessing for Landsat data

For image classification involving algorithm generalization across time, atmospheric correction is required to normalize radiometric measures for images acquired from different years (Furby & Campbell, 2001; Song et al., 2001). A large number of atmospheric correction procedures have been developed: dark object subtraction (DOS) approaches (Chavez, 1988), the histogram matching using pseudo-invariant features (Collins & Woodcock, 1996; Furby & Campbell, 2001), scene-to-scene linear regression (Schott, Salvaggio, and Volchok 1988; Xian, Homer, and Fry 2009; Yang, Xian, *et al.* 2003), and advanced radiative transfer model corrections (Gemmell et al., 2001). In per-pixel image classification and change detection studies, Song (2001) found that simple atmospheric correction method such as DOS outperformed more advanced atmospheric correction algorithms (*e.g.*, radiative transfer corrections). Similar results were reported by many other researchers (Coppin & Bauer, 1994; Gemmell et al., 2001; Pax-Lenney et al., 2001). The main argument is that the success of classification generalization depends on an equivalence of radiometric measurement levels among time-series remote sensing data, rather than correction to standard reflectance units for each image (Schmidt et al., 2013; Song et al., 2001).

For Landsat data, some atmospheric correction algorithms have been integrated by Landsat Ecosystem Disturbance Adaptive Processing System (LEDAPS, http://ledapsweb.nascom.nasa.gov/) to provide ready-to-use surface reflectance images. LEDAPS uses dense vegetation targets as dart objects within the given Landsat scene to extract aerosol optical thickness as input to the 6S radiative transfer model correction (Masek et al.,

2006; Schmidt et al., 2013). LEDAPS, however, may not provide robust surface reflectance estimates for arid and semi-arid regions where vegetation canopies are sparse. Our implementation of LEDAPS resulted in large variations of surface reflectance values across time, which was not suitable for our sub-pixel vegetation mapping purpose, especially with regard to temporal generalization of mapping algorithm.

Based on these previous studies and trials, we implemented a simple DOS correction method to normalize Landsat radiometric measures across time. Song (2001) summarized four specific DOS approaches involving different assumptions of atmospheric transmittance and diffuse irradiance. We followed their DOS1 approach to retrieve surface reflectance (ρ) (Moran et al., 1992; Song et al., 2001):

$$\rho = \frac{\pi(L_{sat} - L_p)}{(E_0 cos(\theta_z))} \quad (1)$$

where L_{sat} is the at-satellite radiance. L_p is the path radiance. E_0 is the exoatmospheric solar constant. θ_z is the solar zenith angle. DOS1 assumes no atmospheric transmittance loss and diffuse downward at the surface. Path radiance (L_p) was estimated using a minimum digital number (DN with at least 1000 pixels) for each image (Chavez, 1996; McDonald, Gemmell, & Lewis, 1998; Teillet & Fedosejevs, 1995). DOS1 corrections were applied to all four Landsat images.

2.3.4 High resolution reference image for sub-pixel vegetation mapping

The OrbView-3 multispectral image was co-registered with the 2004 Landsat image. We conducted a maximum likelihood image classification for the Orbview-3 multispectral image. Initial image classification scheme included eight classes: dry land vegetation, paddy land vegetation, high albedo impervious surface, low albedo impervious surface, high turbidity water, low turbidity water, desert, and barren soil. These preliminary classes were grouped into two

broad classes: vegetation and non-vegetation. Vegetation class includes dry land vegetation and paddy land vegetation. Non-vegetation class includes all the remaining classes (Table 3). Using a stratified random sampling approach, we selected 800 pixels for accuracy assessment of the OrbView-3 image classification. We visually interpreted these 800 points using the OrbView-3 panchromatic and multispectral images as reference. Classification error matrix and kappa statistics were generated to report the image classification accuracy.

The resultant vegetation cover map (4-m spatial resolution) from OrbView-3 classification was rescaled to 30-m grid to spatially match the Landsat pixel resolution. Vegetation proportions were calculated for each 30-m grid. This proportional vegetation map allowed us to generate a large number of training data points for sub-pixel vegetation mapping using Landsat data.

2.3.5 Sub-pixel mapping using Landsat data

We used RF algorithm to generate sub-pixel vegetation maps. The initial RF model was developed using 2004 Landsat spectral signals as input. Vegetation proportions derived from 2004 OrbView-3 image were used as the target variable (Figure 4). We adopted a random sampling strategy to generate training and validation data points. To evaluate the impacts of training sample size on the classification performance, we generated a number of training datasets with varying sample sizes: 100, 200, 1000, 2000, 3000, 4000, and 5000. At each sample size, 20 repeated samplings were conducted to evaluate the variability. For each dataset, a two-fold cross-validation was used for RF training and validation.

The accuracies of RF models were assessed using a root mean squared error (RMSE) statistical measure. The RMSE is calculated as:

$$RMSE = \sqrt{\frac{\sum_{i=1}^{n}(E_i - A_i)^2}{n}}, \quad (2)$$

Where E_i is the predicted vegetation proportion from RF model, A_i is the actual vegetation proportion from the reference vegetation map generated from the OrbView-3 image, and n is the number of sample points used for validation. The accuracy levels of RF models were compared against training/validation sample sizes.

The RF model with the smallest RMSE was retained for subsequent spatial and temporal generalization. Specifically, the best RF model obtained for 2004 Landsat sub-pixel mapping was directly used to classify all other Landsat images from 1990, 1996, and 2011. We anticipated a good generalizability across time given successful image normalization through DOS method described above.

The accuracy of 2011 sub-pixel vegetation mapping was assessed using the concept of "pseudo-invariant' pixels. Supported by Google earth image and local knowledge, we visually identified 250 "pseudo-invariant" pixels where no significant land cover change occurred during 2004 to 2011 (Figure 5). Pseudo-invariant areas included non-vegetated to fully-vegetated area: desert, bare mountain, the Yellow River, core urban area (*e.g.*, older/stable residential blocks). These "pseudo-invariant" pixels" served as our validation data points for 2011 sub-pixel vegetation mapping. We compared proportional vegetation cover predicted from 2004 and 2011 image. Consistent vegetation fractions between 2004 and 2011 were expected for these "pseudo-invariant" pixels".

2.3.6 Vegetation dynamics

Vegetation dynamics were evaluated at both the sub-pixel and per-pixel levels. The image differences between every two vegetation fractional maps provided percent vegetation change per pixel. With predefined thresholds for level of change (*e.g.*, 50% vegetation cover

change), such fuzzy representation of vegetation change maps were also converted to per-pixel vegetation change maps.

To better quantify the spatiotemporal patterns of vegetation changes for the city, we developed an arbitrary mask for specifying the city boundary at the beginning of our study period (1990). We used the 1990 vegetation map rather than using an administrative boundary, to develop the city mask. It comprises the city area within the periphery of vegetation cover, excluding major water bodies (Yellow River). This vegetation mask represented the initial condition of vegetation cover and the initial extent of human habitat during our study period. The patterns of vegetation changes inside/outside of the city boundary were quantified separately for different time-periods.

2.4 Results

The quality of OrbView-3 image classification can have large impacts on the development of a 30-m vegetation proportional map and subsequent sub-pixel vegetation mapping using Landsat images. Per-pixel (4-m spatial resolution) classification of Orbview-3 image needs to have sufficient accuracy to represent the vegetation distribution (*e.g.*, reference image). The overall accuracy of classification is about 71.0%, and the Cohen's Kappa is 0. 6686. Among all eight land cover classes, the high turbidity water surface (the Yellow River) has the highest classification accuracy, while the low albedo impervious surface representing rural built-ups has the lowest accuracy (Table 4). The high producer's accuracy (100%) and very low user's accuracy (53.0%) of low turbidity water suggest an overestimation. On the contrary, the low producer's accuracy (77.4%) and high user's accuracy (90%) of dry land vegetation indicate an underestimation. This overestimation or underestimation mainly resulted from misallocation of paddy land vegetation (rice fields) pixels. In the rice transplanting period, the spectral signature

of paddy land vegetation is similar to those from water surfaces, due to its water background and low vegetation density. Meanwhile, there were strong spectral confusions between deserts and urban surfaces. These spectral confusions indicate a potential difficult in extracting urban impervious surface.

When the eight land cover classes were grouped to two broad cover types (vegetation and non-vegetation), the overall accuracy increased to 93.8% (kappa = 0.8442). The producer's and user's accuracy for vegetation cover were 81.0% and 98.8%, respectively (Table 5). This level of accuracy was sufficient to generate a proportional vegetation map at coarser spatial scale (*i.e.*, 30-m) to serve as training and validation data for Landsat-based sub-pixel vegetation mapping.

2.4.1 Sub-pixel mapping using Landsat data

For sub-pixel mapping using 2004 Landsat image, Figure 6 illustrates the general relationship between the training sample size and classification performance. For each sample size (*e.g.*, 100), we repeated the random data selection 20 times, the medium and range of the resultant RMSE values are depicted. The average RMSE value decreased from 0.16 to 0.10 when the training sample size increased from 100 to 5,000. The variability of RMSE values was also much higher when small number of training sample points were used as training. For example, RMSE ranged from 0.121 to 0.199 when 100 training data points were used. At 5,000 training data points, the range of RMSE values decreased (0.096–0.101). We also noted that the classification achieved the optimum overall performance when 3,000 data points were used as training set, a further increase of sample points did not improve the classification performance. The sample size of 3,000 only accounts for approximately 1.5% of entire reference data. This indicated a possibility of achieving high accuracy of sub-pixel classification with RF algorithm

using relatively small number of training samples, even though a larger number of training data points were available.

In a comparison of the fractional vegetation map generated from Orbview-3 and the Landsat image (Figure 7), scatterplots were generated for 30-m (Figure 7a) and 90-m (Figure 7b) spatial resolutions. A large scatter of the data points is apparent at 30-m pixel comparison. If the Orbview-3 derived fractional vegetation map is considered as true vegetation distribution at the ground, Landsat-estimated sub-pixel vegetation map may have as much as ±30% errors for pixels with intermediate level (*e.g.*, 50%) of vegetation fractions, although the overall accuracy (RMSE = 0.098) is still acceptable due to good classification performance for many pixels with extreme high/low (*e.g.*, 100% or 0%) vegetation cover. One possible reason for the large uncertainty is the possible error of co-registration and the direct comparison at 30-m spatial resolution would then not be recommended (Song 2005). When the fractional vegetation maps were aggregated and compared at 90-m spatial resolution, the level of point scattering was largely reduced and the RMSE value decreased to 0.051. We note that that scatter plots fall in the vicinity of a 1:1 line, which is appealing for unbiased estimation of total vegetation area for the study region.

The RF classifier with the highest cross-validation accuracy was applied to the 1990, 1996, and 2011 images to generate corresponding sub-pixel vegetation cover maps. An initial visual interpretation of the vegetation maps (Figure 8) shows consistent spatial patterns of vegetation cover. A total number of 250 "pseudo-invariant" pixels representing major land cover and land use in the study area were identified. We compared the differences between the estimated vegetation fractions from 2004 and 2011. The RMSE of 0.0506 indicated overall consistent predictions of vegetation fractions for these invariant pixels, suggesting a very good

generalizability of RF sub-pixel classification algorithm across time (Figure 9). The temporal generalizations for other years were assumed to be reliable, as the image normalization and classification procedures were applied consistently.

2.4.2 Vegetation dynamics from 1990 to 2011

In 1990, vegetation cover was dense and cohesively distributed within the irrigated plain as large interconnected field patches. Vegetation distribution at this time provided a clear boundary differentiating urban/human settlement and deserts. We used the 1990 vegetation map to generate an arbitrary urban/human settlement boundary (Figure 10) and assessed trends of vegetation change patterns for areas inside and outside of the boundary. The vegetation changes within and beyond the boundary resulted from two different human activities: urbanization and revegetation.

Within the urban boundary, vegetation cover decreased over the study period (1990–2011) by 16.9% (210.18–174.69 km^2). Outside the boundary, vegetation cover increased by 243.6% (30.69–105.45 km^2) over the same period (Figure 11, Table 6). The revegetation process outside the city proper started in the mid-1990s. From 1990 to 1996, 13.08 km^2 of barren desert were converted to vegetation cover around the city fringe. From 1996 to 2004, more revegetation (36.41km^2) occurred at the city periphery along with some reclamation of desertified mountains on the north edge of the city. From 2004 to 2011, an area of 25.27 km^2 was revegetated, mostly in the northwestern industrial zone of the city.

While the changes in land cover varied spatially over the study period, the total change in vegetated areas in the entire study region increased only slightly across the study period from 240.87 km^2 in 1990 to 280.14 km^2 in 2011, as a result of revegetation programs. We derived three maps illustrating vegetation cover change for three time-periods (1990–1996, 1996–2004

and 2004–2011) at sub-pixel level. The contrasting colors indicate vegetation increase/decrease within each time-period (Figure 12). A threshold value of 0.5 (vegetation fraction) was applied to convert these fuzz representations to vegetation per-pixel change maps.

Within the city boundary (Figure 13a-c), the trajectory of vegetation change shows a clear tendency of urban expansion. From 1990 to 1996, pixels with decreased vegetation cover are mainly scattered in rural areas, reflecting a booming development of villages and small towns. From 1996 to 2004, decreases in vegetation mainly occurred near the urban center and parallel to major roads indicating expansion of the urban core and new road construction, along with human activities along the roads. The most dramatic vegetation change occurred during the period 2004–2011, with northward urban expansion toward the Yellow River and the emergence of new road networks across the city and along the Yellow River.

2.5 Discussion

2.5.1 Subpixel vegetation cover mapping with RF algorithm

In vegetation cover mapping, the Random Forest (RF) algorithm performed well in estimating sub-pixel vegetation proportions for urban core, suburban and urban-desert interface settings. For urban core and suburban areas, vegetation and impervious cover are often mixed within the Landsat pixels. In the urban-desert interface in Zhongwei City, revegetation programs have been implemented, but newly developed vegetation cover (trees or artificial grasslands) could be sparse and mixed with the desert background. We found fractional vegetation cover could be estimated with reasonable accuracy using RF algorithm even though it mixed with different cover types (*e.g.*, impervious surfaces and sand in desert).

We observed some important advantages of the RF classifier during the model implementation. First, a relatively small number (~3,000) of training sample was needed to

achieve strong classification performance. Second, it was easy to implement and only required two parameter adjustments: the number of classification trees, and the number of random split variables used in each node to make the tree grow. Third, when it was combined with a simple atmospheric correction method such as DOS1, RF showed impressive generalization capability across time. The generalizability across time is particularly useful since we could extend this algorithm to additional Landsat images (*e.g.*, Landsat 8) and continue monitoring vegetation dynamics in the future. This strategy would save much time and effort in obtaining additional high resolution vegetation map as training (Yang et al. 2003). In addition, based on available Landsat images and use of appropriate atmospheric correction techniques like DOS, it might be feasible to apply the RF model developed in this study to the nearby cities located in this arid region. For example, cities such as Qingtongxia and Zhongning have very similar geographic settings with our study area. All of these cities are located at the edge of desert and experiencing similar land cover change processes.

Unlike most urban expansion studies in which impervious surface was used as the key index to quantify urban dynamics (*e.g.*, Ji & Jensen, 1999; Lu & Weng, 2006; Wu & Murray, 2003), we used sub-pixel vegetation cover dynamics to characterize human activities in an oasis city of northwest China. Certain impervious surfaces and deserts have similar spectral signals, thus it can be difficult to generate accurate impervious surface map products in this arid setting. A change detection technique that depends solely on impervious cover mapping would lead to large uncertainties. On the other hand, we found that within the initial city boundary (1990), the two major land cover components are impervious surface and vegetation cover; thus the change of vegetation cover could be used as a surrogate to quantify urbanization processes. Vegetation change beyond the initial city boundary was mainly associated with revegetation programs;

however, vegetation changes both within and beyond the initial city boundary were human-induced—one reduced vegetation cover and the other increased vegetation cover. Fractional vegetation cover appeared to be effective in measuring both urbanization and revegetation processes.

2.5.2 Vegetation dynamics in Zhongwei across two decades

Looking at areas within the initial 1990 city boundary we found that urban development showed varied patterns through time. Generally, the change characteristics for the three time-periods can be described as: burgeoning suburban development (1990–1996), extensive infrastructure construction (1996–2004), and urban southward expansion (2004–2011). From 1990 to 1996, most urban development took place in the suburban area rather than the urban core area, represented as extensive development of villages and small towns. From 1996 to 2004, the urban core expanded eastward, accompanying an intensive development of urban infrastructure, especially railways and major roads. These east-west transportation routes promoted an elongated urban expansion along them. From 2004 to 2011, Zhongwei turned into a prefecture-level city from a county, urban development occurred at an increasing rate. The expansion of urban core area shifted from east to south, moving toward the fertile riparian area near the Yellow River, and a series of highways and state roads were constructed. The spatial pattern of newly built-up areas formed a geometry that was mainly been shaped by road networks. During this recent time-period, further development of suburban areas occurred in the east, characterized by massive constructions of greenhouse and related facilities over prime farmland.

The revegetated area at the city fringe has been increasing over time. During 1990s, most of the new vegetation cover appearing along the desert-urban boundary resulted from long-term revegetation programs. Funded by the central government (Yang et al., 2010), these revegetation

programs incorporated a "shelterbelt" (buffer zone protection) system, afforestation, and straw check-board barriers to halt desert encroachment around the city and recover desertified land to productive uses. Since the 21st century, a booming market economy brought new industrial parks at the northern edges. For example, the MCC Meili Paper Industry Park was established to reclaim desert to woodland for pulp and paper production. These irrigated woodlands account for the majority of new vegetation cover starting around 2004.

Oasis cities in northwest China are characterized by many constraints and problems. Many of oasis cities are experiencing desertification, urbanization, vegetation degradation, and population growth (Rashed & Jürgens, 2010). The efforts and achievements in preventing desertification and desert rehabilitation in Zhongwei have been globally acclaimed. In this study, we found a total increase of 74.76 km^2 vegetation coverage at the city edge, but we also observed a substantial decrease in arable lands that were converted to urban (35.49 km^2). Thus, the new revegetated surface areas in deserts were offset by the vegetation loss to development in urban core and suburban areas such that vegetation cover in the study area was reasonably stable (only slightly increased) over time. However, a substitution of desert vegetation for fertile land points to degradation (possibly severe) of vegetation cover. Such substitution along with debatable land use practices such as massive construction of greenhouse over farmland, and large irrigated afforestation in sterile desertified area (Cao, 2008), could result in severely degradation of the quality of vegetation cover in the long run. Our study suggested a regional-scale analysis were needed to measure the actual changes in total vegetation cover through time.

Illustrated through our study, we argue that further research on urbanization and revegetation processes could be beneficial for sustainable development in arid and semi-arid regions in northwestern China. Our study area (*e.g.*, a desert oasis) is confined by limited

resources, but is presently supporting an increasing population. A balance between economic efficiency and ecological benefit should be considered by the government, planners, and land managers of urban development. Land use policies and practices related to urbanization should be based on ongoing and accurate monitoring of land use/cover, to provide a basis for conservation strategy and policy-decisions.

2.6 Conclusion

In this case study for Zhongwei City in northwest China, we derived sub-pixel vegetation fractions from Landsat TM images from 1990, 1996, 2004, and 2011 to support vegetation change analysis. For the year 2004, we used high resolution OrbView-3 image to generate high-resolution vegetation map. The high resolution vegetation map was then used as training data for Landsat-based (2004) sub-pixel vegetation mapping. RMSE value for the 2004 classification was 0.098. We found that a simple atmospheric correction method (DOS1) was effective in normalizing radiometric measures from multiple Landsat scenes across time. The RF algorithm, combined with simple DOS, showed good generalization capability for sub-pixel vegetation mapping. Predicted sub-pixel vegetation proportions were consistent for "Pseudo-invariant" pixels (RMSE = 0.05). Overall, we found our methodology successful in documenting vegetation dynamics in a desert urban environment, illustrating the complexities of human interventions in a fragile environment, and providing useful insights for future urban planning in oasis cities in arid zones in China and possibly elsewhere.

Vegetation change analysis suggested persistent urban development within the initial (1990) city boundary from 1990–2011, accompanied by a continuous expansion of revegetated area at the city fringe over the same time period. A detailed pattern analysis of vegetation dynamics revealed that urban development occurred at both the suburban and urban core areas,

and was mainly shaped by transportation networks. We also documented a transition in revegetation practices: the large-scale governmental revegetation programs were replaced by the commercial afforestation conducted by industries. This study showed only a slight increase in vegetation cover over the time period, balanced by losses to urban expansion, and perhaps most importantly, a likely severe degradation of vegetation cover in Zhongwei due to conversion of arable land to desert vegetation. The loss of arable land and the growth of artificial desert vegetation have yielded a dynamic equilibrium in terms of overall vegetation cover during 1990 to 2011, but in the long run vegetation quality is certainly reduced.

References

Adams, J. B., Sabol, D. E., Kapos, V., Almeida Filho, R., Roberts, D. A., Smith, M. O., & Gillespie, A. R. (1995). Classification of multispectral images based on fractions of endmembers: Application to land-cover change in the Brazilian Amazon. *Remote Sensing of Environment*, *52*(2), 137–154. doi:10.1016/0034-4257(94)00098-8

Adams, J. B., Smith, M. O., & Johnson, P. E. (1986). Spectral mixture modeling: A new analysis of rock and soil types at the Viking Lander 1 Site. *Journal of Geophysical Research: Solid Earth*, *91*(B8), 8098–8112. doi:10.1029/JB091iB08p08098

Akar, Ö., & Güngör, O. (2013). Classification of multispectral images using Random Forest algorithm. *Journal of Geodesy and Geoinformation*, *1*(2), 105–112.

Blaschke, T., Lang, S., Lorup, E., Strobl, J., & Zeil, P. (2000). Object-oriented image processing in an integrated GIS/remote sensing environment and perspectives for environmental applications. *Environmental Information for Planning, Politics and the Public*, *2*, 555–570.

Botkin, D. B., Estes, J. E., MacDonald, R. M., & Wilson, M. V. (1984). Studying the Earth's Vegetation from Space. *BioScience*, *34*(8), 508–514. doi:10.2307/1309693

Bovolo, F., Bruzzone, L., & Carlin, L. (2010). A Novel Technique for Subpixel Image Classification Based on Support Vector Machine. *Image Processing, IEEE Transactions on*, *19*(11), 2983–2999. doi:10.1109/TIP.2010.2051632

Brazel, A., Selover, N., Vose, R., & Heisler, G. (2000). The tale of two climates-Baltimore and Phoenix urban LTER sites. *Climate Research*, *15*(2), 123–135.

Breiman, L. (1999). *Random forests-random features* (No. Technical Report 567). Berkeley, CA: Department of Statistics, University of California.

Breiman, L. (2001). Random Forests. *Machine Learning*, *45*(1), 5–32. doi:10.1023/A:1010933404324

Cao, S. (2008). Why Large-Scale Afforestation Efforts in China Have Failed To Solve the Desertification Problem. *Environmental Science & Technology*, *42*(6), 1826–1831. doi:10.1021/es0870597

Chan, J. C.-W., & Paelinckx, D. (2008). Evaluation of Random Forest and Adaboost tree-based ensemble classification and spectral band selection for ecotope mapping using airborne

hyperspectral imagery. *Remote Sensing of Environment*, *112*(6), 2999–3011. doi:10.1016/j.rse.2008.02.011

Chander, G., Markham, B. L., & Barsi, J. A. (2007). Revised Landsat-5 thematic mapper radiometric calibration. *Geoscience and Remote Sensing Letters, IEEE*, *4*(3), 490–494.

Chavez, P. S. (1988). An improved dark-object subtraction technique for atmospheric scattering correction of multispectral data. *Remote Sensing of Environment*, *24*(3), 459–479. doi:10.1016/0034-4257(88)90019-3

Chavez, P. S. (1996). Image-based atmospheric corrections-revisited and improved. *Photogrammetric Engineering and Remote Sensing*, *62*(9), 1025–1035.

Chen, Y., & Tang, H. (2005). Desertification in north China: background, anthropogenic impacts and failures in combating it. *Land Degradation & Development*, *16*(4), 367–376. doi:10.1002/ldr.667

Collins, J. B., & Woodcock, C. E. (1996). An assessment of several linear change detection techniques for mapping forest mortality using multitemporal landsat TM data. *Remote Sensing of Environment*, *56*(1), 66–77. doi:10.1016/0034-4257(95)00233-2

Coppin, P. R., & Bauer, M. E. (1994). Processing of multitemporal Landsat TM imagery to optimize extraction of forest cover change features. *Geoscience and Remote Sensing, IEEE Transactions on*, *32*(4), 918–927. doi:10.1109/36.298020

Cutler, D. R., Edwards Jr, T. C., Beard, K. H., Cutler, A., Hess, K. T., Gibson, J., & Lawler, J. J. (2007). Random forests for classification in ecology. *Ecology*, *88*(11), 2783–2792.

Elmore, A. J., Mustard, J. F., Manning, S. J., & Lobell, D. B. (2000). Quantifying Vegetation Change in Semiarid Environments: Precision and Accuracy of Spectral Mixture Analysis and the Normalized Difference Vegetation Index. *Remote Sensing of Environment*, *73*(1), 87–102. doi:10.1016/S0034-4257(00)00100-0

Feng, W., Fan, Xu., Lu, T., & Feng, W. (Eds.). (1998). *Zhongwei Yearbook 1994-1995* (Chinese Edition.). Yinchuan: Ningxia People's Publishing House.

Foody, G. M., & Cox, D. P. (1994). Sub-pixel land cover composition estimation using a linear mixture model and fuzzy membership functions. *International Journal of Remote Sensing*, *15*(3), 619–631. doi:10.1080/01431169408954100

Fullen, M. A., & Mitchell, D. J. (1994). Desertification and reclamation in north-central China. *Ambio*, 131–135.

Furby, S. L., & Campbell, N. A. (2001). Calibrating images from different dates to “like-value” digital counts. *Remote Sensing of Environment*, *77*(2), 186–196. doi:10.1016/S0034-4257(01)00205-X

Gemmell, F., Varjo, J., & Strandstrom, M. (2001). Estimating forest cover in a boreal forest test site using Thematic Mapper data from two dates. *Remote Sensing of Environment*, *77*(2), 197–211. doi:10.1016/S0034-4257(01)00206-1

Gislason, P. O., Benediktsson, J. A., & Sveinsson, J. R. (2006). Random Forests for land cover classification. *Pattern Recognition in Remote Sensing (PRRS 2004)*, *27*(4), 294–300. doi:10.1016/j.patrec.2005.08.011

Han, D., & Meng, X. (1999). Recent progress of research on Oasis in China. *Chinese Geographical Science*, *9*(3), 199–205. doi:10.1007/s11769-999-0044-x

Homer, C., Huang, C., Yang, L., Wylie, B. K., & Coan, M. (2004). Development of a 2001 national land-cover database for the United States.

Hung, M.-C., & Ridd, M. K. (2002). A subpixel classifier for urban land-cover mapping based on a maximum-likelihood approach and expert system rules. *Photogrammetric Engineering and Remote Sensing*, *68*(11), 1173–1180.

Ichoku, C., & Karnieli, A. (1996). A review of mixture modeling techniques for sub-pixel land cover estimation. *Remote Sensing Reviews*, *13*(3-4), 161–186. doi:10.1080/02757259609532303

Ji, M., & Jensen, J. R. (1999). Effectiveness of Subpixel Analysis in Detecting and Quantifying Urban Imperviousness from Landsat Thematic Mapper Imagery. *Geocarto International*, *14*(4), 33–41. doi:10.1080/10106049908542126

Jiang, L. (Ed.). (2004). *China Central Western Area Development Yearbook* (Chinese Edition.). Beijing: China Financial and Economic Publishing House. Retrieved from http://book.chaoxing.com/ebook/read_11377869.html

Liang, S., Fallah-Adl, H., Kalluri, S., J áJ á, J., Kaufman, Y. J., & Townshend, J. R. G. (1997). An operational atmospheric correction algorithm for Landsat Thematic Mapper imagery over the

land. *Journal of Geophysical Research: Atmospheres*, *102*(D14), 17173–17186. doi:10.1029/97JD00336

Lin, W., & Chen, T. P. (2004). China's widening economic disparities and its "Go West Program." *Journal of Contemporary China*, *13*(41), 663–686. doi:10.1080/1067056042000281422

Liu, Y. (2012). Analysis of Current Situation in Land Utilization in Shapotou District of Zhongwei Municipality. *Ningxia Journal of Agriculture and Forestry Science and Technology*, *53*(11), 129–130.

Lu, D., & Weng, Q. (2004). Spectral mixture analysis of the urban landscape in Indianapolis with Landsat ETM+ imagery. *Photogrammetric Engineering and Remote Sensing*, *70*(9), 1053–1062.

Lu, D., & Weng, Q. (2006). Use of impervious surface in urban land-use classification. *Remote Sensing of Environment*, *102*(1–2), 146–160. doi:10.1016/j.rse.2006.02.010

Ma, Q. (2004). Appraisal of Tree Planting Options to Control Desertification: Experiences from Three-North Shelterbelt Programme. *International Forestry Review*, *6*(3-4), 327–334. doi:10.1505/ifor.6.3.327.59972

Ma, Y., Fan, S., Zhou, L., Dong, Z., Zhang, K., & Feng, J. (2007). The temporal change of driving factors during the course of land desertification in arid region of North China: the case of Minqin County. *Environmental Geology*, *51*(6), 999–1008. doi:10.1007/s00254-006-0369-z

Masek, J. G., Vermote, E. F., Saleous, N. E., Wolfe, R., Hall, F. G., Huemmrich, K. F., … Lim, T.-K. (2006). A Landsat surface reflectance dataset for North America, 1990-2000. *Geoscience and Remote Sensing Letters, IEEE*, *3*(1), 68–72.

McDonald, A. . J., Gemmell, F. M., & Lewis, P. E. (1998). Investigation of the Utility of Spectral Vegetation Indices for Determining Information on Coniferous Forests. *Remote Sensing of Environment*, *66*(3), 250–272. doi:10.1016/S0034-4257(98)00057-1

McGwire, K., Minor, T., & Fenstermaker, L. (2000). Hyperspectral Mixture Modeling for Quantifying Sparse Vegetation Cover in Arid Environments. *Remote Sensing of Environment*, *72*(3), 360–374. doi:10.1016/S0034-4257(99)00112-1

Mitchell, D. J., Fullen, M. A., Trueman, I. C., & Fearnehough, W. (1998). Sustainability of reclaimed desertified land in Ningxia, China. *Journal of Arid Environments*, *39*(2), 239–251. doi:10.1006/jare.1998.0396

Moran, M. S., Jackson, R. D., Slater, P. N., & Teillet, P. M. (1992). Evaluation of simplified procedures for retrieval of land surface reflectance factors from satellite sensor output. *Remote Sensing of Environment*, *41*(2–3), 169–184. doi:10.1016/0034-4257(92)90076-V

Nalepka, R. F., & Hyde, P. D. (1972). Classifying unresolved objects from simulated space data. In *Proceedings of the Eighth International Symposium on Remote Sensing of Environment* (Vol. 2, pp. 935–949). Environmental Research Institute of Michigan,Ann Arbor, Michigan. Retrieved from http://ntrs.nasa.gov/search.jsp?R=19730055080

Nicholson, S. E., Tucker, C. J., & Ba, M. B. (1998). Desertification, Drought, and Surface Vegetation: An Example from the West African Sahel. *Bulletin of the American Meteorological Society*, *79*(5), 815–829. doi:10.1175/1520-0477(1998)079<0815:DDASVA>2.0.CO;2

Orbital Imaging Corporation. (2006). *OrbView-3: Fact sheet*. Dulles, VA: Orbital Sciences Corporation. Retrieved from http://www.orbital.com/newsinfo/publications/ov3_fact.pdf

Pal, M. (2005). Random forest classifier for remote sensing classification. *International Journal of Remote Sensing*, *26*(1), 217–222. doi:10.1080/01431160412331269698

Pax-Lenney, M., Woodcock, C. E., Macomber, S. A., Gopal, S., & Song, C. (2001). Forest mapping with a generalized classifier and Landsat TM data. *Remote Sensing of Environment*, *77*(3), 241–250. doi:10.1016/S0034-4257(01)00208-5

Phinn, S., Stanford, M., Scarth, P., Murray, A. T., & Shyy, P. T. (2002). Monitoring the composition of urban environments based on the vegetation-impervious surface-soil (VIS) model by subpixel analysis techniques. *International Journal of Remote Sensing*, *23*(20), 4131–4153. doi:10.1080/01431160110114998

Powell, R. L., Roberts, D. A., Dennison, P. E., & Hess, L. L. (2007). Sub-pixel mapping of urban land cover using multiple endmember spectral mixture analysis: Manaus, Brazil. *Remote Sensing of Environment*, *106*(2), 253–267. doi:10.1016/j.rse.2006.09.005

Prasad, A. M., Iverson, L. R., & Liaw, A. (2006). Newer Classification and Regression Tree Techniques: Bagging and Random Forests for Ecological Prediction. *Ecosystems*, *9*(2), 181–199. doi:10.1007/s10021-005-0054-1

Qi, S. Z., Li, X. Y., & Duan, H. P. (2007). Oasis land-use change and its environmental impact in Jinta Oasis, arid northwestern China. *Environmental Monitoring and Assessment*, *134*(1-3), 313–320. doi:10.1007/s10661-007-9622-5

Rashed, T., & Jürgens, C. (Eds.). (2010). *Remote sensing of urban and suburban areas*. Dordrecht ; London: Springer.

Ridd, M. K. (1995). Exploring a V-I-S (vegetation-impervious surface-soil) model for urban ecosystem analysis through remote sensing: comparative anatomy for cities. *International Journal of Remote Sensing*, *16*(12), 2165–2185. doi:10.1080/01431169508954549

Rodriguez-Galiano, V. F., Ghimire, B., Rogan, J., Chica-Olmo, M., & Rigol-Sanchez, J. P. (2012). An assessment of the effectiveness of a random forest classifier for land-cover classification. *ISPRS Journal of Photogrammetry and Remote Sensing*, *67*(0), 93–104. doi:10.1016/j.isprsjprs.2011.11.002

Schmidt, G., Jenkerson, C., Masek,, J., Vermote,, E., & Gao, F. (2013). *Landsat Ecosystem Disturbance Adaptive Processing System (LEDAPS) Algorithm Description* (No. Open-File Report 2013–1057) (p. 27). Reston, Virginia: U.S. Geological Survey. Retrieved from http://pubs.usgs.gov/of/2013/1057/ofr13_1057.pdf

Schneider, A., Seto, K. C., & Webster, D. R. (2005). Urban growth in Chengdu, Western China: application of remote sensing to assess planning and policy outcomes. *Environment and Planning B: Planning and Design*, *32*(3), 323–345.

Schott, J. R., Salvaggio, C., & Volchok, W. J. (1988). Radiometric scene normalization using pseudoinvariant features. *Remote Sensing of Environment*, *26*(1), 1–16. doi:10.1016/0034-4257(88)90116-2

Settle, J. J., & Drake, N. A. (1993). Linear mixing and the estimation of ground cover proportions. *International Journal of Remote Sensing*, *14*(6), 1159–1177. doi:10.1080/01431169308904402

Shalaby, A., Ghar, M. A., & Tateishi, R. (2004). Desertification impact assessment in Egypt using low resolution satellite data and GIS. *International Journal of Environmental Studies*, *61*(4), 375–383. doi:10.1080/0020723042000199740

Shalaby, A., & Tateishi, R. (2007). Remote sensing and GIS for mapping and monitoring land cover and land-use changes in the Northwestern coastal zone of Egypt. *Applied Geography*, *27*(1), 28–41. doi:10.1016/j.apgeog.2006.09.004

Shao, X. (2011). *Study on artificial forest dynamics using object-based image analysis at Shapotou District, Zhongwei City, Ningxia Autonomous Region* (Master Thesis). Lanzhou University, Lanzhou, China. Retrieved from http://cdmd.cnki.com.cn/Article/CDMD-10730-1012373169.htm

Shao, Y., & Lunetta, R. S. (2012). Comparison of support vector machine, neural network, and CART algorithms for the land-cover classification using limited training data points. *ISPRS Journal of Photogrammetry and Remote Sensing*, *70*(0), 78–87. doi:10.1016/j.isprsjprs.2012.04.001

Shi, P.-J., Shimizu, H., Wang, J.-A., Liu, L.-Y., Li, X.-Y., Fan, Y.-D., … Song, Y. (2005). Land degradation and blown-sand disaster in China. In K. Omasa, I. Nouchi, & L. Kok (Eds.), *Plant Responses to Air Pollution and Global Change* (pp. 261–269). Tokyo: Springer Japan. Retrieved from http://dx.doi.org/10.1007/4-431-31014-2_29

Small, C. (2001). Estimation of urban vegetation abundance by spectral mixture analysis. *International Journal of Remote Sensing*, *22*(7), 1305–1334. doi:10.1080/01431160151144369

Smith, M. O., Ustin, S. L., Adams, J. B., & Gillespie, A. R. (1990). Vegetation in deserts: II. Environmental influences on regional abundance. *Remote Sensing of Environment*, *31*(1), 27–52. doi:10.1016/0034-4257(90)90075-W

Sobrino, J. A., Jiménez-Muñoz, J. C., & Paolini, L. (2004). Land surface temperature retrieval from LANDSAT TM 5. *Remote Sensing of Environment*, *90*(4), 434–440. doi:10.1016/j.rse.2004.02.003

Song, C. (2005). Spectral mixture analysis for subpixel vegetation fractions in the urban environment: How to incorporate endmember variability? *Remote Sensing of Environment*, *95*(2), 248–263. doi:10.1016/j.rse.2005.01.002

Song, C., Woodcock, C. E., Seto, K. C., Pax-Lenney, M., & Macomber, S. A. (2001). Classification and Change Detection Using Landsat TM Data: When and How to Correct Atmospheric Effects? *Remote Sensing of Environment*, *75*(2), 230–244. doi:10.1016/S0034-4257(00)00169-3

State Forestry Administration, P. R. China. (2011). *A Bulletin of Status Quo of Desertification and Sandification in China*.

Statistical Bureau of Ningxia Hui Autonomous Region, & Survey Office of the National Bureau of Statistics in Ningxia Hui Autonomous Region (Eds.). (2012). *Ningxia Statistical Yearbook*. Beijing, China: China Statistics Press.

Su, Y. Z., Zhao, W. Z., Su, P. X., Zhang, Z. H., Wang, T., & Ram, R. (2007). Ecological effects of desertification control and desertified land reclamation in an oasis–desert ecotone in an arid region: A case study in Hexi Corridor, northwest China. *Ecological Engineering*, *29*(2), 117–124. doi:10.1016/j.ecoleng.2005.10.015

Teillet, P. M., & Fedosejevs, G. (1995). On the dark target approach to atmospheric correction of remotely sensed data. *Canadian Journal of Remote Sensing*, *21*(4), 374–387.

Thornton, M. W., Atkinson, P. M., & Holland, D. A. (2006). Sub-pixel mapping of rural land cover objects from fine spatial resolution satellite sensor imagery using super-resolution pixel-swapping. *International Journal of Remote Sensing*, *27*(3), 473–491. doi:10.1080/01431160500207088

Tooke, T. R., Coops, N. C., Goodwin, N. R., & Voogt, J. A. (2009). Extracting urban vegetation characteristics using spectral mixture analysis and decision tree classifications. *Remote Sensing of Environment*, *113*(2), 398–407. doi:10.1016/j.rse.2008.10.005

Townshend, J. R. G., Huang, C., Kalluri, S. N. V., Defries, R. S., Liang, S., & Yang, K. (2000). Beware of per-pixel characterization of land cover. *International Journal of Remote Sensing*, *21*(4), 839–843. doi:10.1080/014311600210641

UNDP. (n.d.). Ningxia Anti-desertification and Livelihood Improvement. Retrieved September 18, 2013, from http://www.undp.org/content/china/en/home/operations/projects/environment_and_energy/ningxia-anti-desertification-and-livelihood-improvement-/

USGS. (2012, January 24). OrbView-3. *USGS Long Term Archive*. U.S. Geological Survey. Retrieved January 11, 2014, from https://lta.cr.usgs.gov/satellite_orbview3

Walton, J. T. (2008). Subpixel urban land cover estimation: comparing cubist, random forests, and support vector regression. *Photogrammetric Engineering and Remote Sensing*, *74*(10), 1213–1222.

Wang, S., Ma, Y., Hou, Q., & Wang, Y. (2007). Coping Strategies with Desertification in China. In M. V. K. Sivakumar & R. P. Motha (Eds.), *Managing Weather and Climate Risks in Agriculture* (pp. 317–341). Springer Berlin Heidelberg. Retrieved from http://dx.doi.org/10.1007/978-3-540-72746-0_18

Wang, T., Wu, W., Xue, X., Sun, Q., & Chen, G. (2004). Study of spatial distribution of sandy desertification in North China in recent 10 years. *Science in China Series D: Earth Sciences*, *47*(1), 78–88. doi:10.1360/04zd0009

Wang, X. M., Zhang, C. X., Hasi, E., & Dong, Z. B. (2010). Has the Three Norths Forest Shelterbelt Program solved the desertification and dust storm problems in arid and semiarid China? *Journal of Arid Environments*, *74*(1), 13–22. doi:10.1016/j.jaridenv.2009.08.001

Wu, C., & Murray, A. T. (2003). Estimating impervious surface distribution by spectral mixture analysis. *Remote Sensing of Environment*, *84*(4), 493–505. doi:10.1016/S0034-4257(02)00136-0

Wu, H. (Ed.). (2011). *Zhongwei Yearbook 2010* (Chinese Edition.). Yinchuan: Ningxia People's Publishing House.

Wu, H. (Ed.). (2013). *Zhongwei Yearbook 2012* (Chinese Edition.). Yinchuan: Ningxia People's Publishing House.

Xian, G., Homer, C., & Fry, J. (2009). Updating the 2001 National Land Cover Database land cover classification to 2006 by using Landsat imagery change detection methods. *Remote Sensing of Environment*, *113*(6), 1133–1147. doi:10.1016/j.rse.2009.02.004

Yan, C., Wang, Y., Feng, Y., & Wang, J. (2003). Macro-scale Survey and Dynamic Studies of Sandy Land in Ningxia by Remote Sensing. *Journal of Desert Reserch*, *23*(2), 132–135.

Yang, L., Huang, C., Homer, C. G., Wylie, B. K., & Coan, M. J. (2003). An approach for mapping large-area impervious surfaces: synergistic use of Landsat-7 ETM+ and high spatial resolution imagery. *Canadian Journal of Remote Sensing*, *29*(2), 230–240. doi:10.5589/m02-098

Yang, L., Lan, Z., & Wu, J. (2010). Roles of Scholars in the Practice of Combating-Desertification: A Case Study in Northwest China. *Environmental Management*, *46*(2), 154–166. doi:10.1007/s00267-010-9534-y

Yang, L., Xian, G., Klaver, J. M., & Deal, B. (2003). Urban land-cover change detection through sub-pixel imperviousness mapping using remotely sensed data. *Photogrammetric Engineering and Remote Sensing*, *69*(9), 1003–1010.

Yang S., Taff, G. N., & Walsh, S. J. (2011). Comparison of Early Stopping Criteria for Neural-Network-Based Subpixel Classification. *Geoscience and Remote Sensing Letters, IEEE, 8*(1), 113–117. doi:10.1109/LGRS.2010.2052782

Zhu, Z. (1989). Advance in Desertification Research in China. *Journal of Desert Research, 1*.

Figures and Tables

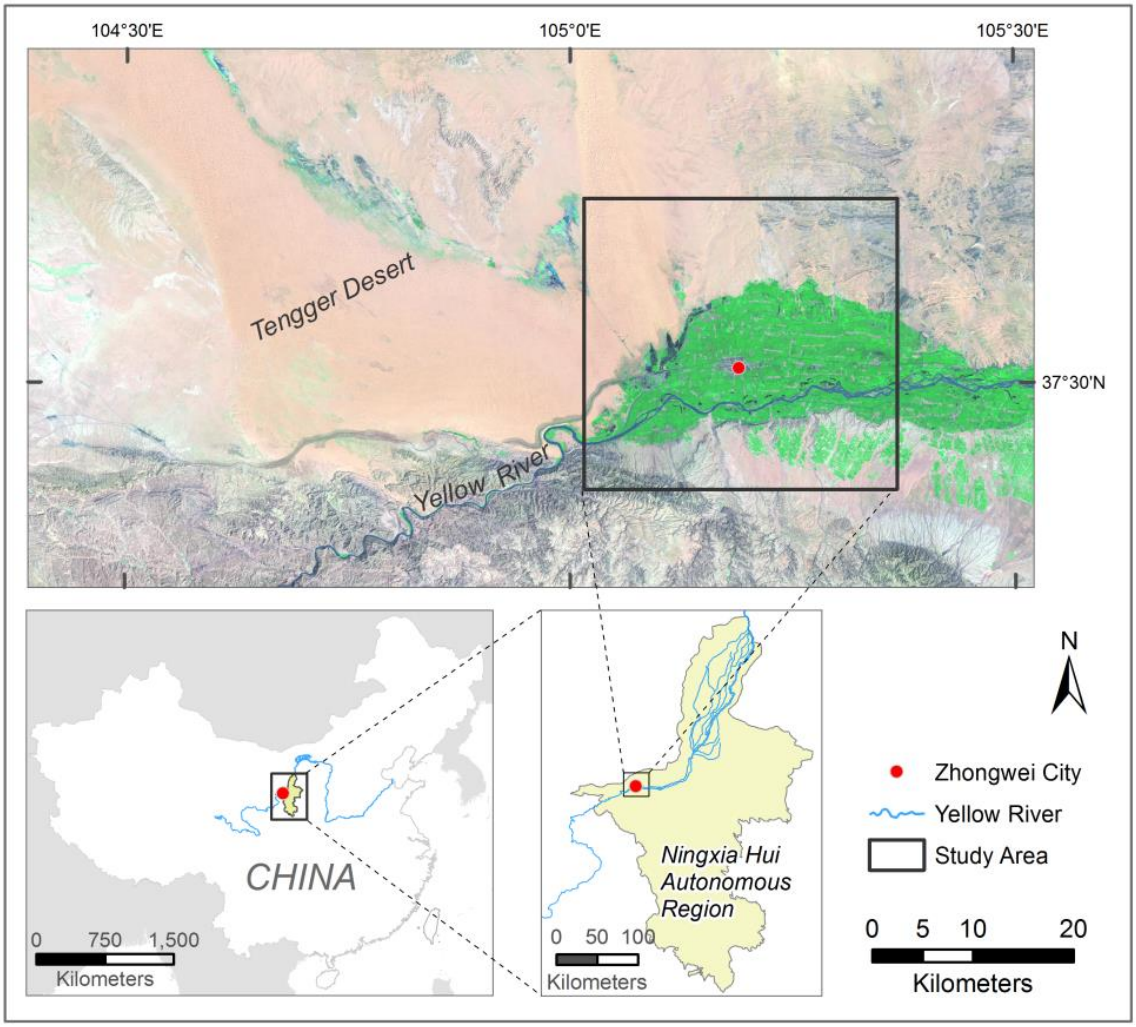

Figure 1. Maps of China and Ningxia Hui Automous Region showing location of Zhongwei city (104.28 º– 105.62 ºE, 36.98 º– 37.72 ºN) in northwestern China. The city lies at the edge of an oasis and abuts the southeastern frontier of the Tengger Desert. The Yellow River traverses the irrigated plain of the city. Zhongwei covers a total area of 16,986 km^2. Over 90% of areas are mountains, loess hilly region, and desert. This study only focused on the city municipal district.

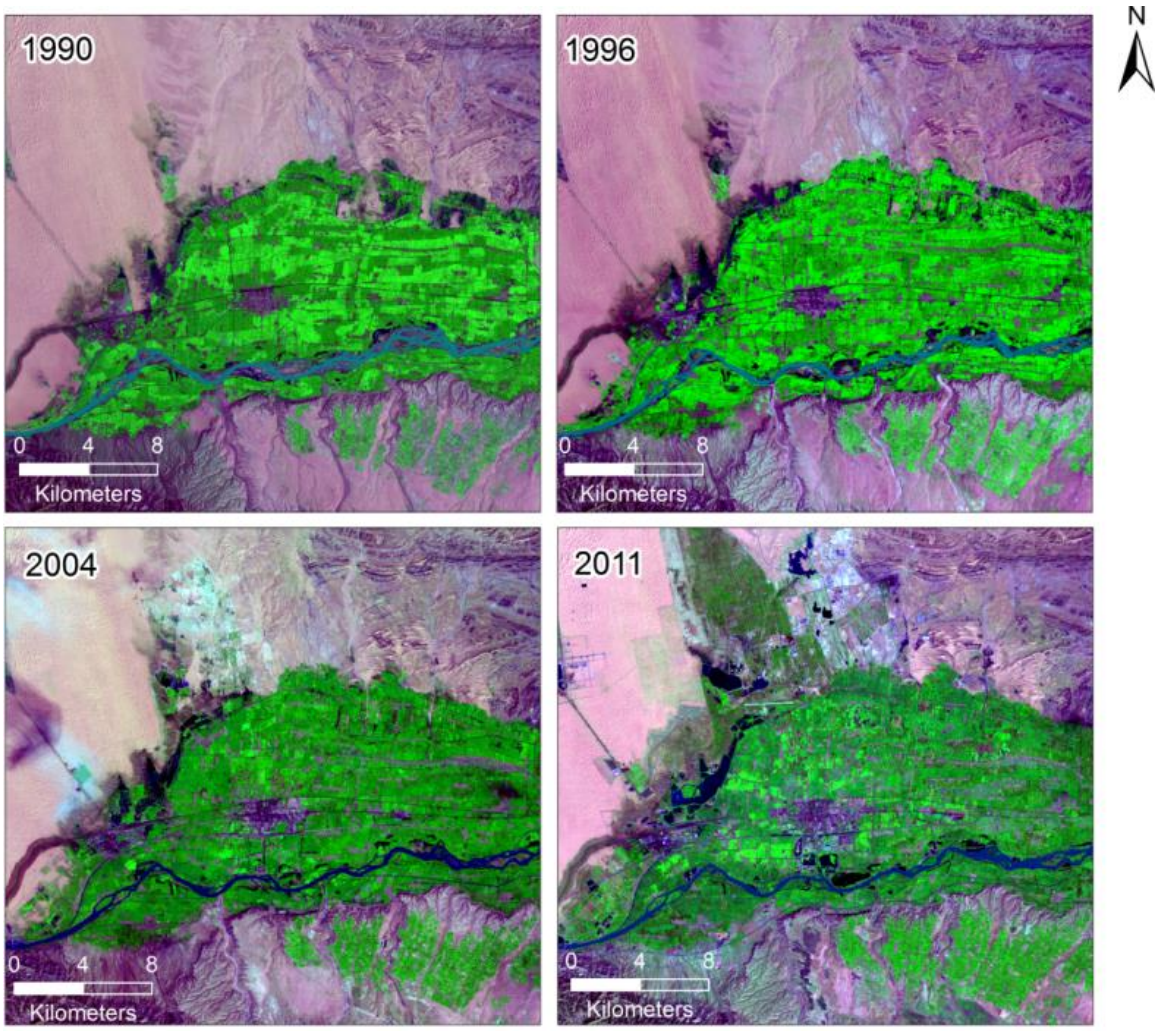

Figure 2. Landsat 5 TM images (1990, 1996, 2004 and 2011, subsetted to study area) used for multi-temporal sub-pixel vegetation mapping. Images are displayed as 7-4-2 band combination.

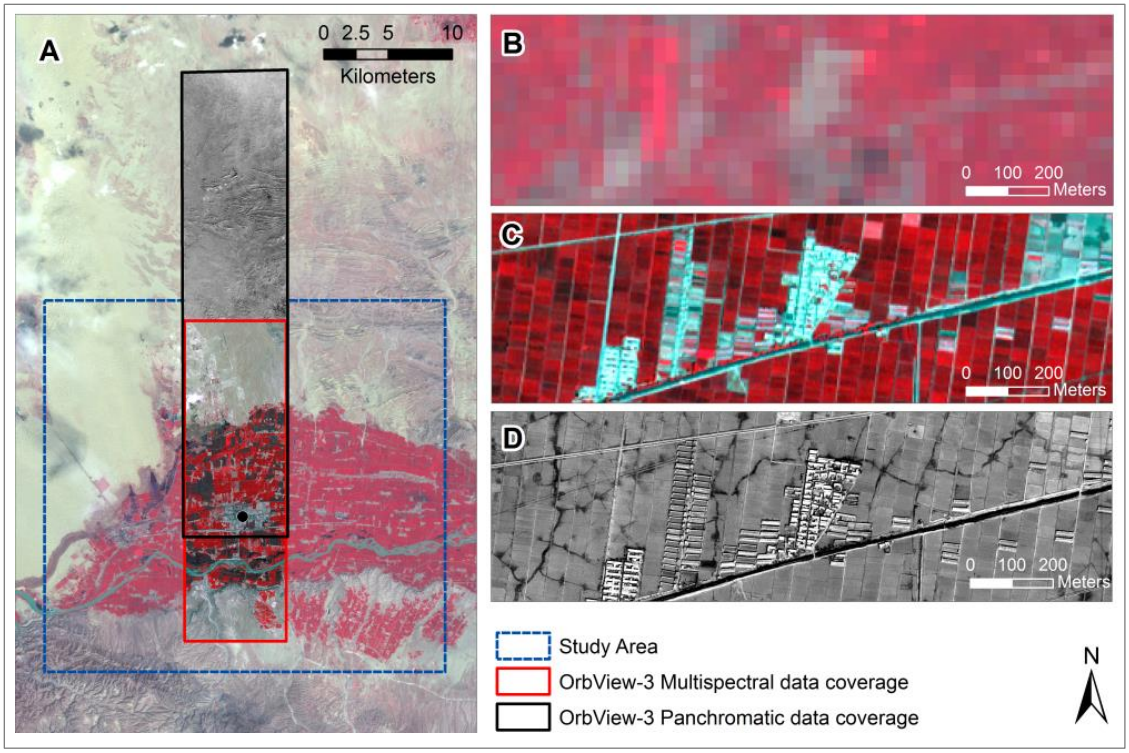

A) Coverage of OrbView-3 multispectral and panchromatic (black-and-white) data. B, C and D) indicate resolutions of Landsat data, OrbView-3 multispectral data and panchromatic data respectively. Multispectral images are displayed in 4-3-2 band combination.

Figure 3. The coverages of OrbView-3 multispectral (4-m resolution) and panchromatic (1-m resolution) high spatial resolution images. The spatial extents of the multispectral and panchromatic images are about 8km x 25km and about 8km x 35km, respectively. The coverages of two images run through Zhongwei city from north to south and have overlap at the urban core area. Both images are of high quality and cloud-free. The OrbView-3 multispectral image was co-registered with the 2004 Landsat image, and was used for developing high resolution reference vegetation map.

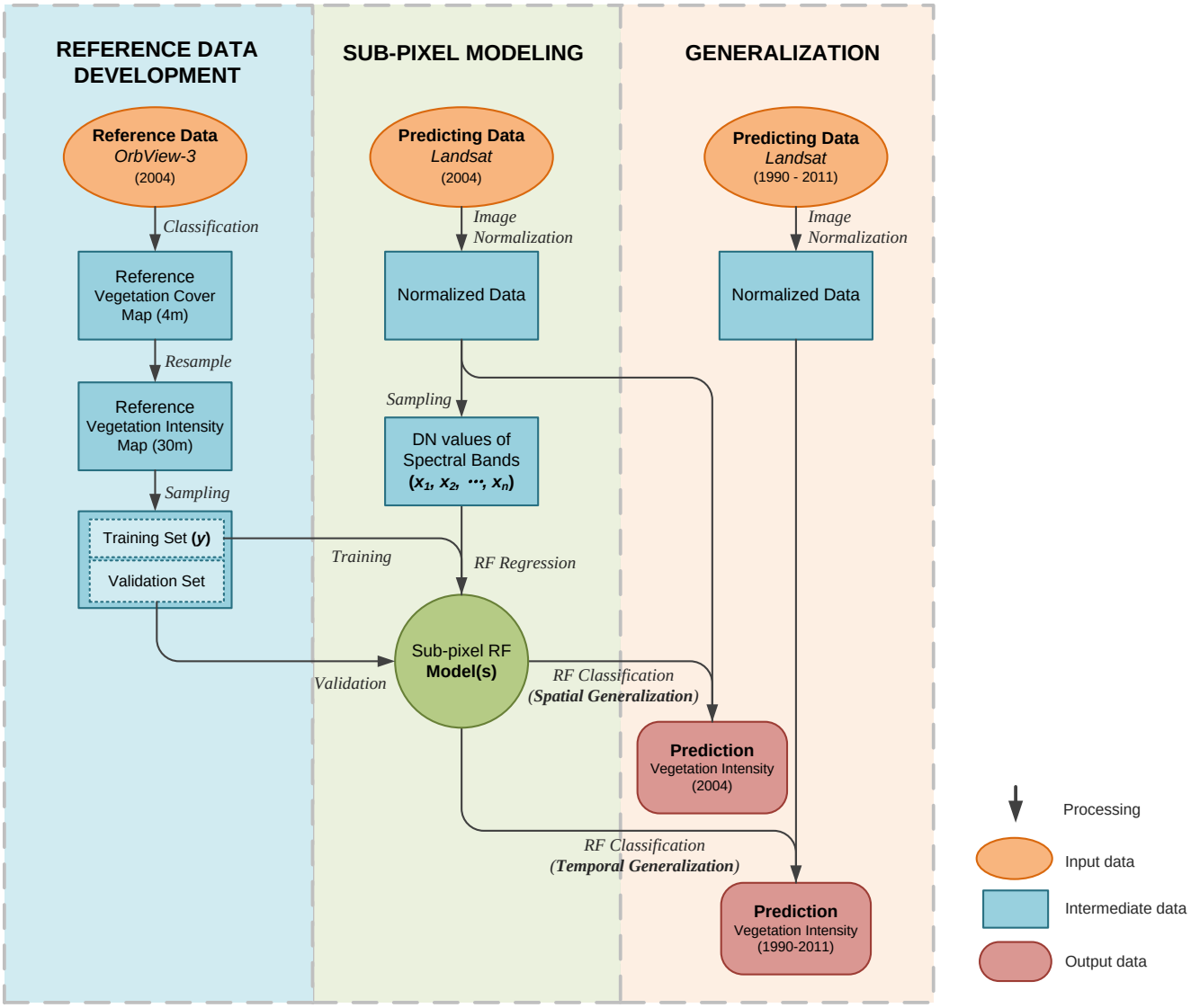

Figure 4. workflow of multi-temporal sub-pixel vegetation mapping with Random Forest algorithm. Three major steps includes: reference data development, sub-pixel vegetation cover mapping with RF algorithm, and classification generalization.

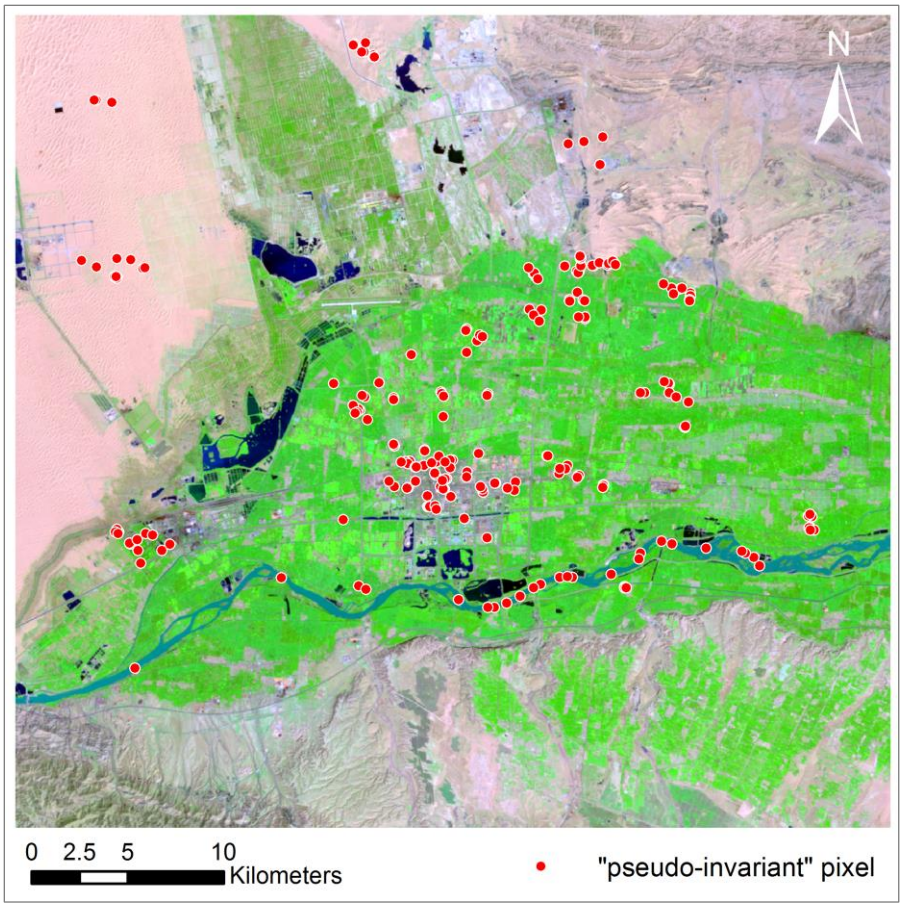

Figure 5. Pseudo-invariant pixels for evaluating temporal generalization of classification of 2011 image. Pseudo-invariant areas included non-vegetated to fully-vegetated area: desert, bare mountain, the Yellow River, core urban area (*e.g.*, older/stable residential blocks). These "pseudo-invariant" pixels served as validation data points for 2011 sub-pixel vegetation mapping. The proportional vegetation covers predicted from 2004 and 2011 images were compared. Consistent vegetation fractions between 2004 and 2011 were expected for these "pseudo-invariant" pixels.

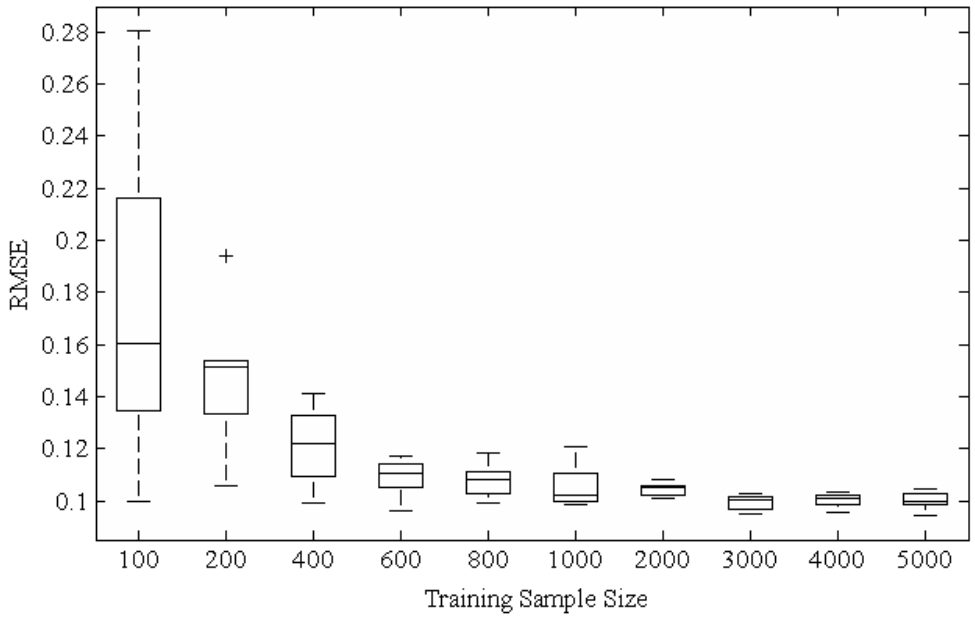

Figure 6. Comparison of classification accuracies of RF classifier (in RMSE) using different training sample sizes. The average RMSE value decreased from 0.16 to 0.10 when the training sample size increased from 100 to 5,000. The classification achieved the optimum overall performance when 3,000 data points were used as training set, a further increase of sample points did not improve the classification performance.

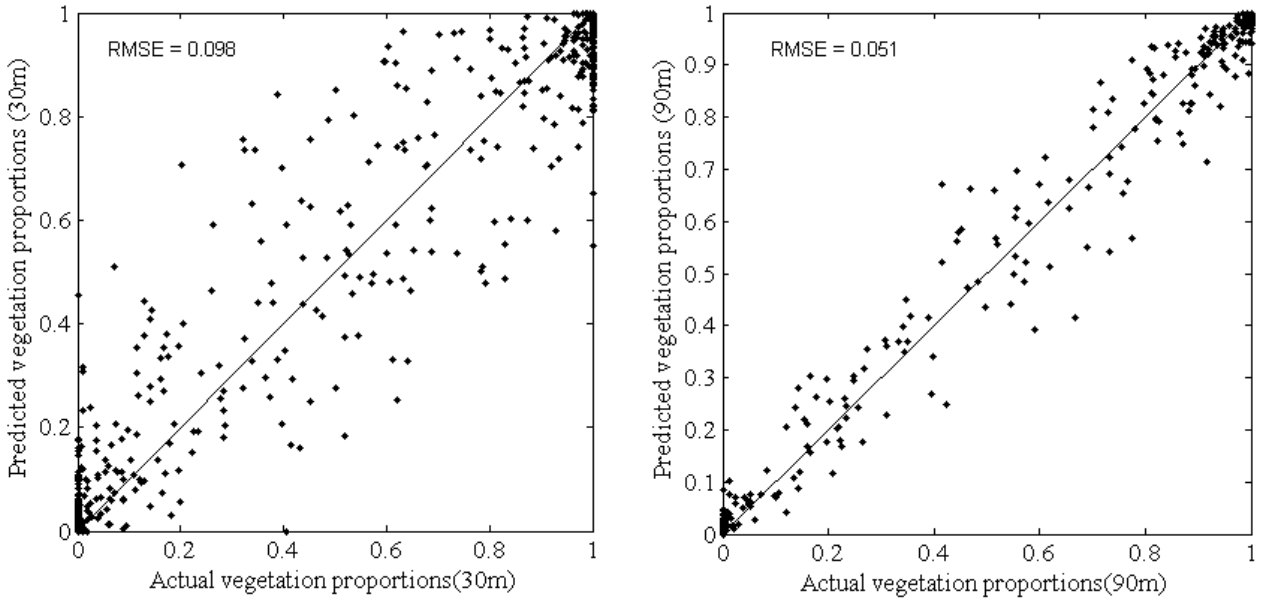

Figure 7. Accuracy assessments of RF classifier used in this study for 30-m and 90-m spatial resolution. The overall accuracy for 30-m spatial resolution (RMSE = 0.098) is acceptable. When the fractional vegetation maps were aggregated and compared at 90-m spatial resolution, the level of point scattering was largely reduced and the RMSE value decreased to 0.051. Both scatter plots fall in the vicinity of a 1:1 line, which is appealing for unbiased estimation of total vegetation area for the study region.

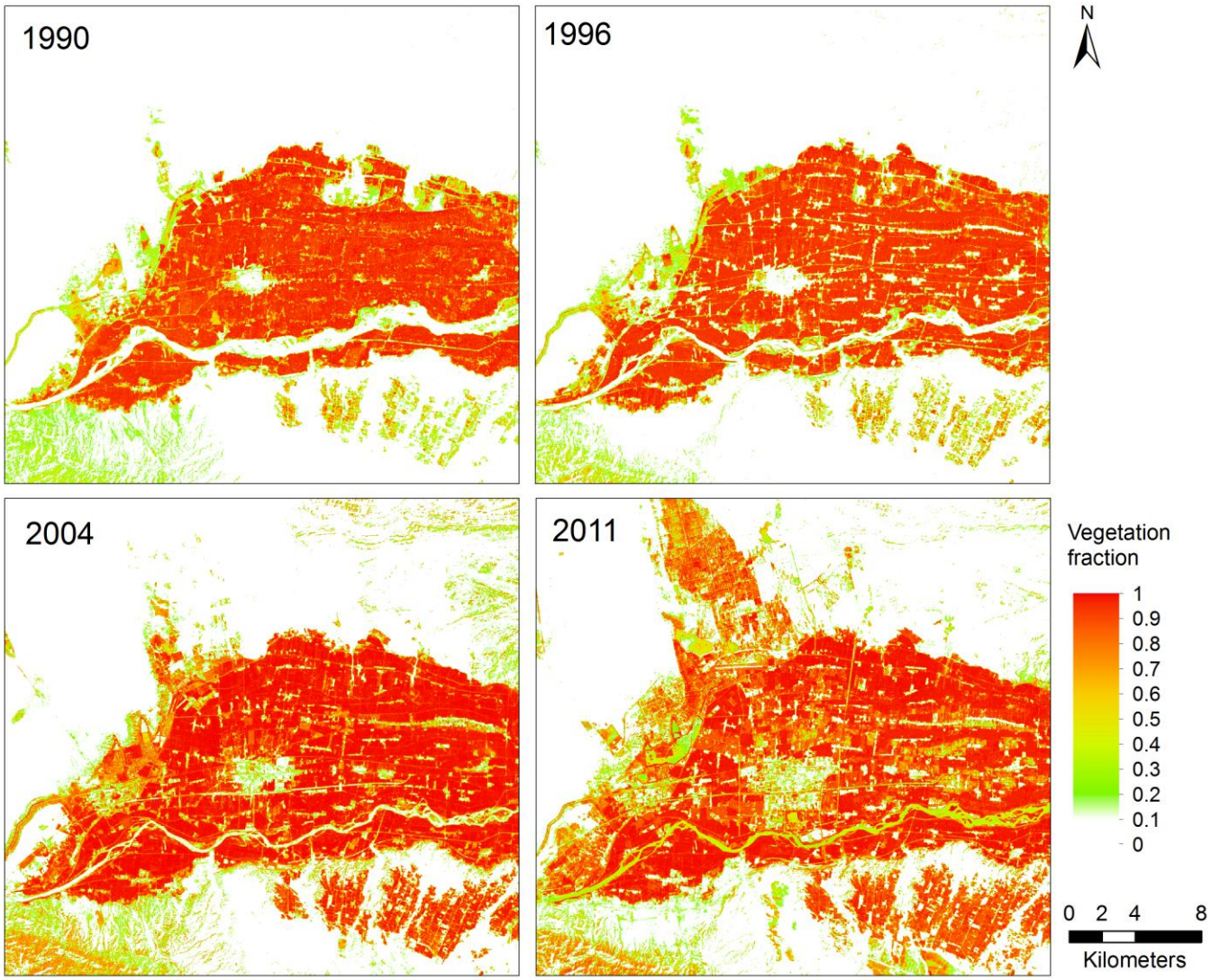

Figure 8. Sub-pixel vegetation cover maps for 1990, 1996, 2004 and 2011. The dark red color indicates high vegetation fraction

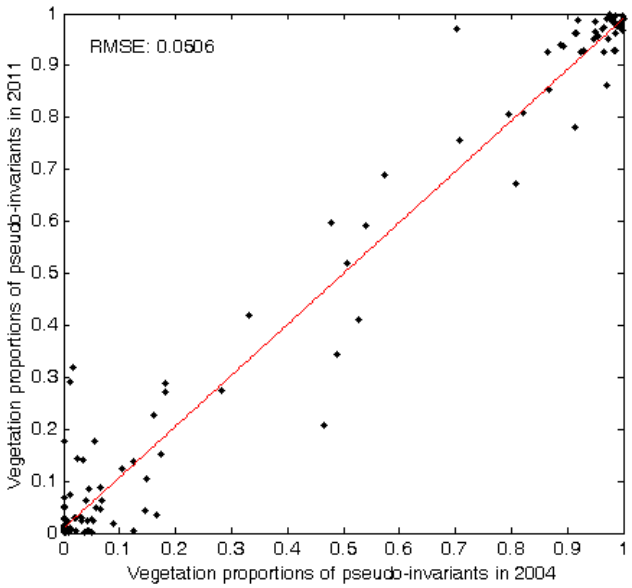

Figure 9. Evaluation of temporal generalization of classification of 2011 image by comparing vegetation proportions of pseudo-invariant pixels between 2004 and 2011. RMSE of 0.0506 indicated overall consistent predictions of vegetation fraction for invariant pixels. It suggested a very good generalizability of RF sub-pixel classification algorithm across time.

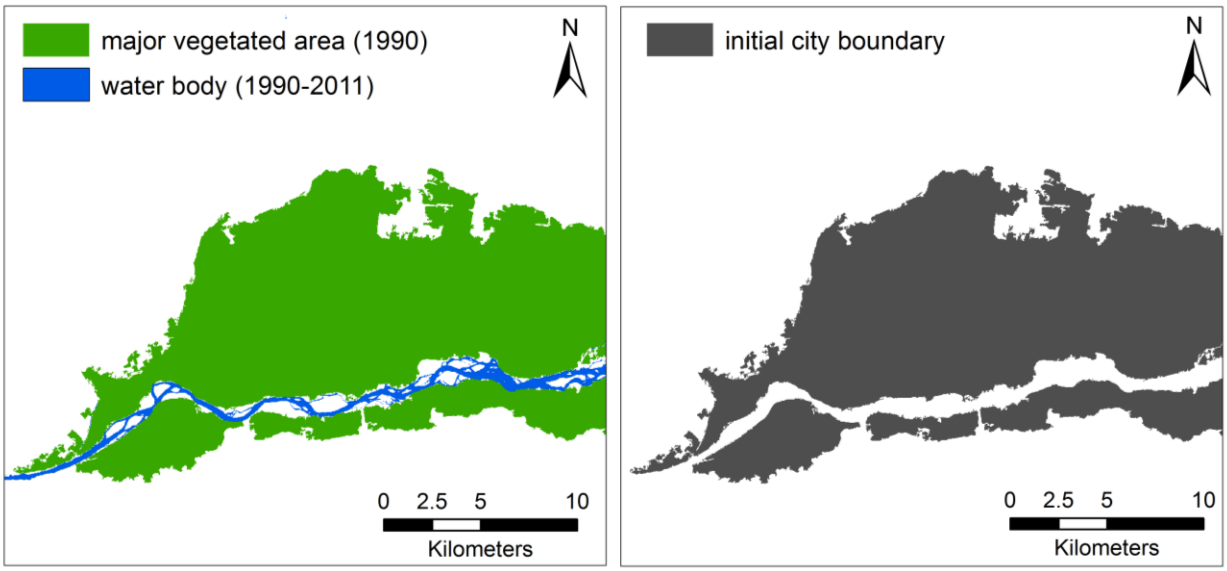

Figure 10. An arbitrary mask for specifying initial (1990) city boundary. The mask comprises the city area within the periphery of vegetation cover, excluding major water bodies (Yellow River). It represented the initial condition of vegetation cover and the initial extent of human habitat during study period. The patterns of vegetation changes inside/outside of the city boundary were quantified separately for different time-periods.

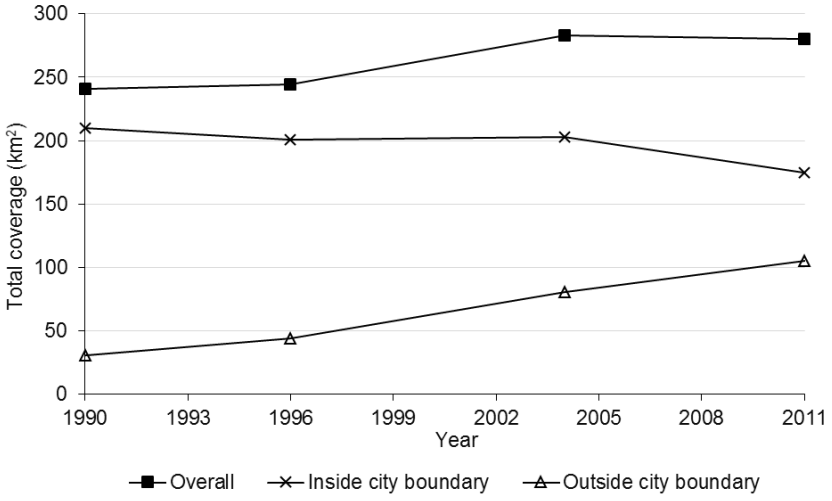

Figure 11. The areas of vegetation cover in 1990, 1996, 2004 and 2011. It suggests a persistent decrease vegetation cover inside city boundary, accompanied by a continuous expansion of vegetation cover outside city boundary. Thus, the new revegetated surface areas in deserts were offset by the vegetation loss to development in urban such that vegetation cover in the study area was reasonably stable (only slightly increased) over time.

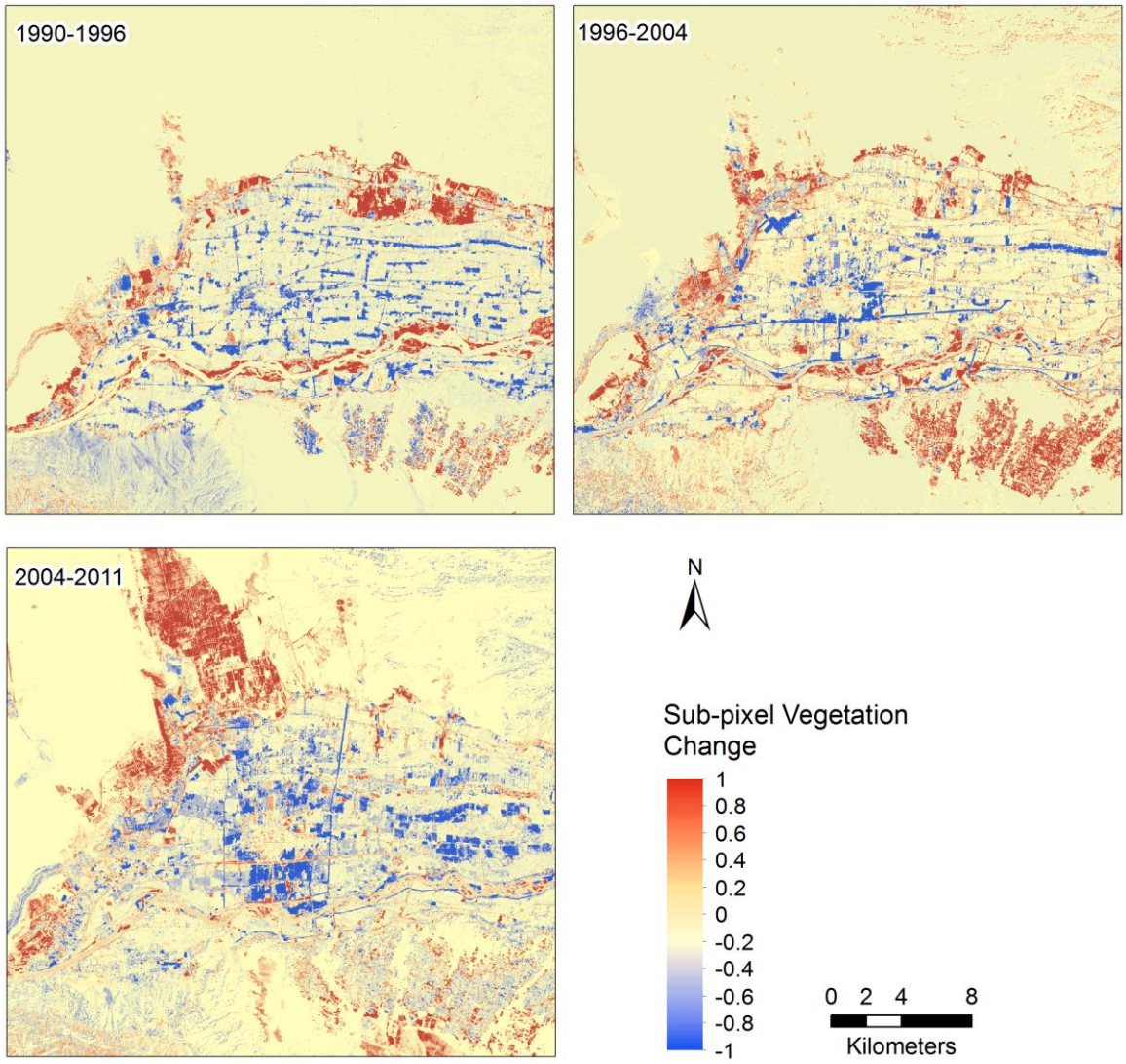

Figure 12. Maps of sub-pixel vegetation change for three time-periods during 1990 to 2011. The red/blue color indicates vegetation increase/decrease within each time-period.

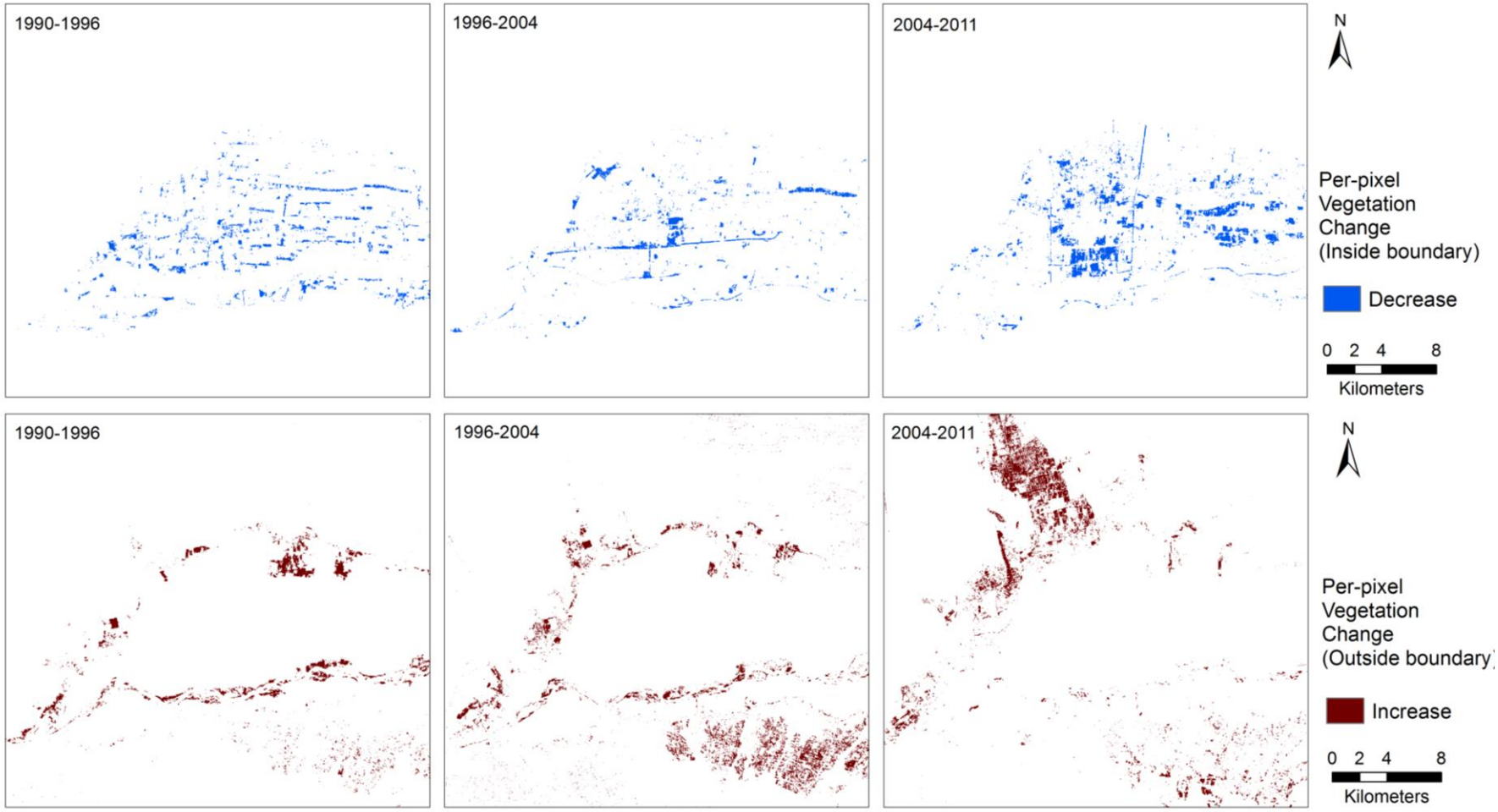

Figure 13. Maps of per-pixel vegetation change inside and outside initial city boundary for three time-periods. A threshold value of 0.5 (vegetation fraction) was applied to convert previous sub-pixel vegetation change maps (figure 12) to this per-pixel vegetation change maps.

Table 1. Landsat 5 TM images (1990, 1996, 2004 and 2011; path 130, row 34) used for sub-pixel vegetation cover mapping. All images derive from USGS EROS Data center.

Scene ID	Acquisition date	Solar zenith angle
LT51300341990230BJC00	8/18/1990	37.19
LT51300341996215BJC00	8/2/1996	35.15
LT51300342004253BJC00	9/9/2004	38.99
LT51300342011240IKR00	8/28/2011	34.96

Table 2. Specifications of Orbview-3 multispectral (4-m resolution) and panchromatic (1-m resolution) images. The multispectral image was used for developing high resolution reference vegetation map, while the panchromatic image was used as reference data for classification of multispectral image.

Orbview3 Entity ID	3V040314P0000312121A520000100362M_001651842	3V040620M0000388871A520000600122M_001667437
Sensor	Panchromatic	Multispectral
Acquisition Date	3/14/2004	6/20/2004
Cloud Cover	none	none
Pixel Size X (meter)	1.03	3.97
Pixel Size Y (meter)	1.03	3.92
Spatial Dimension (km^2)	8.3 x 37.5	8.0 x 25.0
Center Coordination	37.663 ºN, 105.183 ºE	37.539 ºN, 105.184 ºE
Sun Azimuth	151.98	131.26
Sun Elevation	46.06	70.19

Table 3. Classification schemes and description for OrbView-3 high resolution image. The OrbView-3 image was classified into eight classes (Classes II). These preliminary classes were grouped into two broad classes (Class I): vegetation and non-vegetation. Vegetation class includes dry land vegetation and paddy land vegetation. Non-vegetation class includes all the remaining classes.

Classes I	Classes II	Description
Vegetation cover	Dry land vegetation	Cropland, woodland, shrubs, *etc.*
	Paddy land vegetation	Vegetated flooded field, rice land
Non-vegetation cover	High albedo impervious surface	Built-up area in urban center, industrial area
	Low albedo impervious surface	Rural built-up area
	High turbidity water	Yellow River
	Low turbidity water	Lakes, reservoirs, ponds
	Desert	Desert
	Barren	Bare mountains, unutilized bare land

Table 4. Accuracy assessment of OrbView-3 image Classification using the eight-class classification scheme. The overall accuracy of classification is 71.0%, and the Cohen's Kappa is 0. 6686. There were strong spectral confusions between deserts and urban surfaces. These spectral confusions also indicate a potential difficult in extracting urban impervious surface.

		Classification map									
		High turbidity water	Low turbidity water	Dry land vegetation	Paddy land vegetation	Desert	Barren	High albedo impervious surface	Low albedo impervious surface	Total	Producer's accuracy
Reference data	High turbidity water	99	3	0	0	0	0	1	0	103	96.1%
	Low turbidity water	0	53	0	0	0	0	0	0	53	100.0%
	Dry land vegetation	0	6	90	17	2	0	0	6	121	74.4%
	Paddy land vegetation	0	29	10	79	0	1	1	1	121	65.3%
	Desert	0	0	0	1	93	10	19	30	153	60.8%
	Barren	0	0	0	1	3	68	12	32	116	58.6%
	High albedo impervious surface	1	0	0	0	1	4	56	1	63	88.9%
	Low albedo impervious surface	0	9	0	2	1	17	11	30	70	42.9%
	Total	100	100	100	100	100	100	100	100	800	
	User's accuracy	99.0%	53.0%	90.0%	79.0%	93.0%	68.0%	56.0%	30.0%	Overall accuracy 71.0%	

Cohen's kappa = 0.6686

Table 5. Accuracy assessment of OrbView-3 image Classification using the two-class classification scheme. The overall accuracy of classification increased to 93.8%, and the Cohen's Kappa is 0.0.8442. This level of accuracy was sufficient to generate a proportional vegetation map at coarser spatial scale (*i.e.*, 30-m) to serve as training and validation data for Landsat-based sub-pixel vegetation mapping.

		vegetation cover map			
		Vegetation cover	Non-vegetation cover	Total	Producer's accuracy
Reference data	Vegetation cover	196	46	242	81.0%
	Non-vegetation cover	4	554	558	99.3%
	Total	200	600	800	
	User's accuracy	98.0%	92.3%	Overall accuracy 93.8%	

Cohen's kappa = 0.8442

Table 6. Statistics of vegetation coverages in Zhongwei for 1990, 1996, 2004 and 2011.

	Vegetation coverage (km^2)			
	Year 1990	Year 1996	Year 2004	Year 2011
Overall	240.87	244.57	282.74	280.14
Inside city boundary	210.18	200.80	202.56	174.69
Outside city boundary	30.69	43.77	80.18	105.45